WATER BUDGET ANALYSIS AND GROUNDWATER INVERSE MODELING

A Thesis

by

SAYENA FARID MARANDI

Submitted to the Office of Graduate Studies of
Texas A&M University
in partial fulfillment of the requirements for the degree of

MASTER OF SCIENCE

May 2012

Major Subject: Biological and Agricultural Engineering

Water Budget Analysis and Groundwater Inverse Modeling

WATER BUDGET ANALYSIS AND GROUNDWATER INVERSE MODELING

A Thesis

by

SAYENA FARID MARANDI

Submitted to the Office of Graduate Studies of
Texas A&M University
in partial fulfillment of the requirements for the degree of

MASTER OF SCIENCE

Approved by:

Chair of Committee,	Binayak P. Mohanty
Committee Members,	Hongbin Zhan
	Patricia Smith
Head of Department,	Stephen Searcy

May 2012

Major Subject: Biological and Agricultural Engineering

ABSTRACT

Water Budget Analysis and Groundwater Inverse Modeling.

(May 2012)

Sayena Farid Marandi, B.Sc, Iran University of Science & Technology

Chair of Advisory Committee: Dr. Binayak P. Mohanty

The thesis contains two studies: First is the water budget analysis using the groundwater modeling and next is the groundwater modeling using the MCMC scheme. The case study for the water budget analysis was the Norman Landfill site in Oklahoma with a quite complex hydrology. This site contains a wetland that controls the groundwater-surface water interaction. This study reports a simulation study for better understanding of the local water balance at the landfill site using MODFLOW-2000. Inputs to the model are based on local climate, soil, geology, vegetation and seasonal hydrological dynamics of the system to determine the groundwater-surface water interaction, water balance components in various hydrologic reservoirs, and the complexity and seasonality of local/regional hydrological processes. The model involved a transient two- dimensional hydrogeological simulation of the multi-layered aquifer. In the second part of the thesis, a Markov Chain Monte Carlo (MCMC) method were developed to estimate the hydraulic conductivity field conditioned on the measurements of hydraulic conductivity and hydraulic head for saturated flow in randomly heterogeneous porous media.

The groundwater modeling approach was found to be efficient in identifying the dominant hydrological processes at the Norman Landfill site including evapotranspiration, recharge, and regional groundwater flow and groundwater-surface water interaction. The MCMC scheme also proved to be a robust tool for the inverse groundwater modeling but its strength depends on the precision of the prior covariance matrix.

DEDICATION

To my dear parents

and my loving husband, Ardeshir

ACKNOWLEDGEMENTS

I would like to sincerely thank Dr. Binayak Mohanty for his guidance and financial support during this study. I also wish to thank Dr. Hongbin Zhan and Dr. Patricia Smith who freely shared their time with me and for their guidance and insight throughout the course of this research. Gratitude also goes to Dr. Ronald Kaiser and decedent Dr. Valeen Silvy who provided encouragement and financial support during the initial portion of my research work. In addition, I also thank Dr. Istvan Szunyogh from the Atmospheric Science Department, Dr. Sharat Girimaji from the Department of Aerospace Engineering and Behnam Tarrahi from the Department of Petroleum Engineering for providing helpful advice for my research work.

Thanks also go to my friends and colleagues and the department faculty and staff for making my time at Texas A&M University a great experience. I also want to extend my gratitude to the USGS, which provided the valuable data.

Finally, thanks to my mother and father for their encouragement and to my husband for his patience and love.

NOMENCLATURE

USGS	United States Geological Survey
LAI	Leaf Area Index
S_y	Specific Yield
K_h or K_x	Horizontal Hydraulic Conductivity
K_v or K_z	Vertical Hydraulic Conductivity
NRMS	Normalized Root Mean Squared
pdf	probability density function
MCMC	Markov Chain Monte Carlo
ET	Evapotranspiration

TABLE OF CONTENTS

Page

LIST OF FIGURES

Page

LIST OF TABLES

Page

1. INTRODUCTION

Water is the basis of life, and preservation of water and its related ecosystems calls for effective water resource management through a scientific understanding of the processes and interactions in the hydrological cycle. Modern hydrology aims at building a model mimicking the data environment of the unknown processes; that model can be regarded as a collection of numerical techniques that deals with the characterization of spatial and temporal attributes of the hydrological cycle. Computer simulation of groundwater flow is a decision-support, heuristic and predictive tool used to characterize the water flow processes in soils and approximate both conceptual models and boundary conditions. Hence numerical simulation of subsurface water flow has been undertaken to analyze the components of the hydrologic cycle through its process-based capabilities [*Cosner et al.*, 1978; *Lindgren et al.*, 1999; *McDonald et al.*, 1998; *Purdic*, 1989]. Some integrated groundwater/ surface water models also have the ability to provide comprehensive water budget analysis honoring the law of conservation of mass [*Belmans et al.*, 1983; *Markstrom et al.*, 2008].

Many applications of groundwater flow modeling involve water balance analysis at a range of scales. Surface soils react dynamically to the climatic sequence of precipitation and evapotranspiration events. They accept part of the moisture throughout a precipitation event, returning some of it back to the surface during evaporative periods,

---

This thesis follows the style of *Water Resources Research.*

and conduct the remainder to the water table [*Eagleson*, 1978]. The quantitative relationship among the long-term averages of this sequence is called the water balance. When a surface water body, such as a wetland, is included in the domain, the complexity of modeling tends to increase due to the interaction between the surface water and groundwater. Groundwater and surface water are hydraulically interconnected, but most often their interactions are difficult to observe and measure. However, it is possible to quantify the interactions through numerical simulations. Groundwater flow models allow calculation of the boundary flux rates and simulation of the surface water/ groundwater interactions, including where and when the exchanges take place.

Comprehensive hydrogeology analyses are not only imperative for water supply studies, but also provide information to carry out the hydro-bio-geochemical analysis affects fate and transport of contaminants at a location of interest such as a landfill. Transport analysis needs a map of key hydrologic parameters such as hydraulic conductivity and effective porosity in addition to a description of the flow regime in an appropriate resolution [*Eggleston et al.*, 1998; *Zheng et al.*, 2002]. Inability to characterize different dominant processes and property variations completely contributes to uncertainty in flow and transport model analysis. The utilization of a groundwater flow model specific to a complex hydrological site leads to the knowledge of a site's hydrogeology which comes not from the data, but from the model. A by-product of the application of a groundwater model to an intricate case study is to determine if the limitations of the current model call for a far more consequential simulation. In addition to groundwater modeling, inverse problems in groundwater modeling have been also

studied extensively by *Kitanidis et al*.[1983], *Yeh* [1986], *Ginn et al*.[1990] ,*Sun* [1990] , *McLaughlin et al.* [1996] , *Woodbury et al.* [2000], *Wu et al.* [2004] and *Carrera* [2005] to name a few. There are several notable peculiarities in inverse groundwater modeling that have posed a challenge to it and, therefore have attracted a remarkable research effort. These features include the spatial and temporal variability of measured dependent variables such as hydraulic head and solute concentration, different types of parameters (hydraulic conductivity, recharge, boundary fluxes, etc.), scale dependence, model uncertainty such as the geometry of the aquifer and heterogeneity patterns controlled by the geology, nonlinearity , instability (small errors in the dependent variables cause large errors in the parameters) and often low sensitivity of the dependent variables to the aquifer properties [*Carrera et al.*, 2005].

Inverse problems in groundwater modeling require a mathematical model that incorporates variable models and simulate a dependent variable such as hydraulic head or solute concentration at observation points [*McLaughlin et al.*, 1996]. The variable models are hydraulic parameters such as hydraulic conductivity, storativity and porosity over the whole domain of the aquifer. These properties are one of the key parameters in the hydrogeological characterization of the aquifer; however, hydraulic conductivity is the dominant soil physical property [*Woodbury et al.*, 2000]. Because flow rate in the aquifer both upward and downward is governed by the saturated hydraulic conductivity of the soil layer [*Arnold et al.*, 1993] . It has also been widely accepted that the heterogeneity and spatial variability of the hydraulic conductivity controls the flow field and consequently the spread of contaminants. [*Dagan*, 1986; *Gelhar*, 1986; *Woodbury et*

al., 2000]. The role of the hydraulic conductivity becomes more apparent particularly in an investigative modeling framework that allows more insight into the system behavior and hydrological processes.

Hydraulic conductivity is difficult to measure and, therefore, inverse problems are used for its estimation [*McLaughlin et al.*, 1996]. Deterministic and stochastic frameworks are two types of groundwater inverse models. In deterministic models, nonlinear regression type techniques are used to estimate hydraulic properties in such a way that the observation and simulation data fit [*Neuman*, 1973]. The set of equations in this method are highly underdetermined because the number of unknowns is more than the data points. To overcome this problem, additional types of data can be considered as *a priori* information which is the case of the Lavenburg-Marquardt algorithm [*Press et al.*, 1992].

In the stochastic approach, the estimate of hydraulic conductivity, K, is based on geostatistics and is represented as a weighted linear combination of all measurements of hydraulic properties [*Kitanidis*, 1996; *Woodbury et al.*, 2000]. Both deterministic and stochastic approaches treat hydrogeological properties as spatial functions and, thus, there also exist hybrid methods which lie between the two approaches [*McLaughlin et al.*, 1996] .

As an example of the geostatistical approach, in the Cokriging method, the unknown log (K) at any location is solved for by the weighted linear combinations of observed dependent variables [*Kitanidis*, 1996; *Woodbury et al.*, 2000]. The approach requires a linearized relationship between the log (K) and the dependent variables in

order to construct the cross-covariance of the log (K) perturbations. This linearized relationship is valid only if the covariance of log (K) is small [*Woodbury et al.*, 2000]. Accordingly, for highly heterogeneous cases, the Cokriging method cannot take full advantage of pressure head measurements [*Woodbury et al.*, 2000; *Yeh et al.*, 1995].Another drawback of the method is that the dependent variables found using the Cokriging equations in general will not honor their corresponding measurements [*Lu et al.*, 2004]. The latter drawback was improved by the work of *Yeh et al.* [1995] by developing an iterative Cokriging technique which allows sequential updating of hydraulic conductivities in such a way that the modeled head values were close to the observed values within a given error [*Lu et al.*, 2004].

A full Bayesian approach to the estimation of the hydraulic conductivity field using hydraulic head observations and hydraulic conductivity measurements for steady state flow was proposed by *Woodbury et al.* [2000]. In this method, the *a priori* probability density function (pdf) is determined from the maximum entropy method .The approach provides an alternative to the Kriging method for spatial interpolation [*Woodbury et al.*, 2000]. *Lu et al.* [2004] developed a Markov Chain Monte Carlo (MCMC) method for the groundwater inverse problem to estimate the hydraulic conductivity field conditioned on the measurements of hydraulic conductivity and hydraulic head .The MCMC method is one of the most computationally intensive technique which yields a pdf for the set of parameters and does not require difficult assumptions [*Carrera et al.*, 2005]. Therefore ,aquifer characterization using MCMC has attracted much research.

The first objective of this study was to identify the main components of the water budget and the dominant processes controlling the circulation of the water at the closed municipal landfill research site in Norman, Oklahoma.

The second objective was to develop an inverse groundwater model using MCMC that accounts for both the measurements of natural log (K) and head measurements. The proposed approach utilized variogram-based stochastic simulation to obtain the *a priori* pdf of the parameter. The model was tested for a hypothetical 2-D saturated transient flow in a heterogeneous porous medium for which the geology pattern and the boundary conditions were inspired by the hydrogeology of the Norman Landfill site in Oklahoma .

2. GROUNDWATER MODELING

2.1. Site Description

The Norman Landfill Research site is a closed municipal landfill situated on the alluvial aquifer of the Canadian River in Norman, Oklahoma, and also one of the U.S. Geological Survey Toxic Substances Hydrology Program sites. Studies have been undertaken at this research site to describe the interaction of the landfill with the surrounding environment and the effect of natural biodegradation on the leachate plume [*Becker*, 2002; *Eganhouse et al.*, 1999; *Scholl et al.*, 1999]

The hydrologic cycle of the Norman Landfill site is influenced by the small natural wetland referred to as the "slough", as well as by the seasonal variations of evapotranspiration and recharge [*Christenson et al.*, 1999] . The main source of recharge to the wetland is groundwater, including native and leachate-contaminated groundwater, and sub-surface flows resulting from large precipitation events [*Schlottmann et al.*, 1999]. The wetland-aquifer interaction was found to be a complex interface zone between groundwater and surface water as well as a bio-geo-chemical filter for water quality processes [*Baez-Cazull et al.*, 2008] .Groundwater head measurements by the USGS reveal that water levels are lower during the growing season and higher otherwise. The soil, vegetation, atmosphere and wetland systems of the site are dynamically interconnected with each other by means of physical processes driving the energy and water balances.

Although the seasonal hydrological patterns and the linkage between the wetland and the aquifer are believed to influence chemical, biological [*Baez-Cazull et al.*, 2008;

Christenson et al., 1999] and recharge processes [*Scholl et al.*, 2006], there are no published studies dedicated to quantifying the water budget of the site through an investigative hydrological model. Such an investigative study would allow more insight into the system's behavior, yet the prediction may not be as robust as the predictive models [*Bowles et al.*, 1991].

The site accepted solid municipal waste from 1922 to 1985, by which time it was closed and capped with local clay [*Schlottmann et al.*, 1999]. Of particular interest is the 1164 m long a transect referred to as A-A' (Figure 1) in the direction of the groundwater flow. There are 3 water level monitoring wells situated alongside: (1) Well WLMLF, located on the mound of the landfill in the west cell, (2) Well IC36, located 35 m from the edge of the landfill and (3) Well IC54 located 7 m from the down-gradient edge of the wetland (Figure 1).

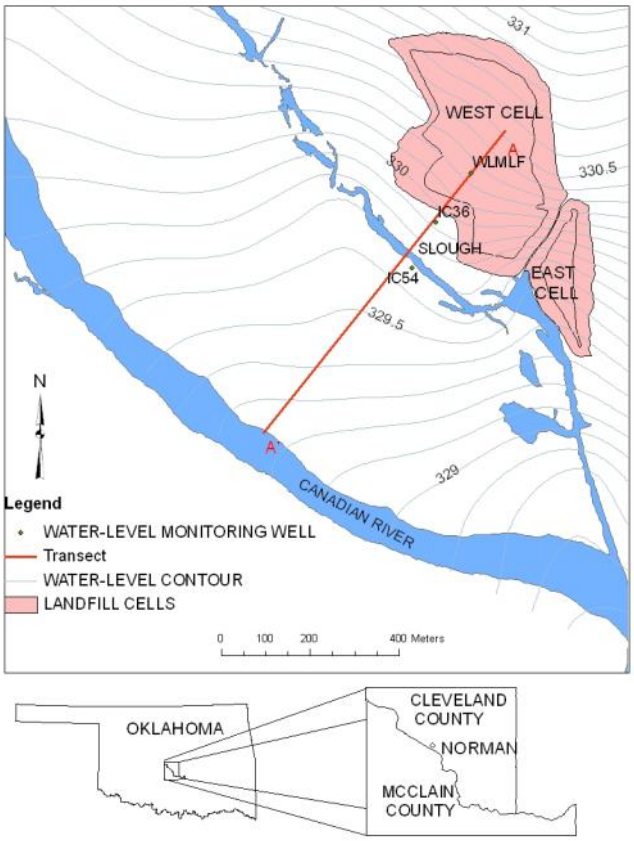

Figure 1. Location of the site, streams, observation wells, transect A-A' and regional potentiometric surface map at Norman Landfill Site, Oklahoma. [*http://ok.water.usgs.gov/projects/norlan/*]

2.1.1. Climatology

Annual precipitation at the site is approximately 96 cm, with rainfall rates greater than potential evapo-transpiration (ET) during spring, summer and fall seasons. The hottest month is July with the average temperature of 28° C and the coldest month is January with the average temperature of 3.5° C [*www.mesonet.com*, 1994]. The growing season starts in mid-April and ends in October [*Scholl et al.*, 2006].

2.1.2. Land Cover

The riparian zone of the wetland is densely vegetated with both deep and shallow rooted plants. The deep-rooted or phreatophyte type of vegetation consists of willow, cottonwood, eastern red cedar and salt cedar while the wetland vegetation includes common reed, western ragweed, bermuda grass, johnson grass, bundle flower, ravenna grass, giant cane, sandbar willow and black willow [*Burgess,* 2006]. It has been shown by *Busch et al.* [1992] that willows as well as salt cedar use only groundwater and exhibit little evidence of water acquisition from the unsaturated zone, while cottonwoods use both soil water and groundwater [*Busch et al*., 1992]. Most of these plants are rooted in the soil and they grow in dense thickets along the wetland.

2.1.3. Recharge

The recharge study in the Norman Landfill Research site over 2 years (1998-2000) conducted by *Scholl et al.* [2006], suggested that recharge to the riparian area is around 16% to 64% of rain events. The wide range of the recharge rate is mainly due to the difference between the chemical and physical methods used in the recharge estimation. Chemical methods involved measuring the change in recharge water in the saturated zone, as defined by isotopic signature, specific conductance or chloride measurements; and infiltration rate estimates using storm event isotopic signatures [*Scholl et al.*, 2006]. Physical methods included measurement of water table rise after each rain event and on an approximately monthly time scale [*Scholl et al.*, 2006]. Isotopes analyses showed that recharge entered the groundwater system in winter

(December 21- March 20) and spring (March 20- June 20), and was removed during the growing season [*Scholl et al.*, 2006].

2.1.4. The Wetland

The wetland is impounded by a beaver dam in the former channel of the Canadian River with a length of approximately 700 m [*Scholl et al.*, 2006] (Figure 2). The wetland has a complex hydrological regime which results from a multifaceted interplay between the climate and aquifer characteristics. Interactions between the groundwater-surface water system may be a dominant component of the water budget since inland wetlands are usually connected with the groundwater system [*Winter,* 1999]. In particular, existence of surface water bodies can strongly affect the hydraulic heads in the surficial aquifers through hydraulic influence and exchanges of water with the atmosphere [*Merritt et al.,* 2000]. The wetland not only has interaction with the atmosphere, it also receives lateral flow from upstream and discharges into a wastewater effluent stream from the City of Norman wastewater treatment plant. The wetland is a surface expression of the water table and it serves both as a source and a sink in the water budget system during wet and dry seasons [*Christenson et al.,* 1999]. It is fed by the groundwater recharge and precipitation during the wet seasons and in the dry periods it is depleted by ET.

Figure 2. The beaver dam that formed the wetland in the Norman Landfill Site. (Photo by Scott Christenson, USGS Toxic Substance Hydrology Program-Norman Landfill Project)

2.1.5. Groundwater Flow System

The groundwater flow system at the site consists of local, intermediate and regional recharge or discharge into/from the domain. The local groundwater flow system gains water at the higher topographies and discharges into immediately adjacent lows, while the regional groundwater system is recharged and discharged at major topographic highs and lows respectively [*Carter,* 1996; *Winter,* 1976]. The intermediate flow system occurs between these two topographic bounds [*Carter,* 1996; *Winter,* 1976] (Figure 3).

In the winter of 1995-1996, a network of shallow temporary wells was constructed in the Canadian River alluvium to create a potentiometric-surface map [*Scholl et al.,* 1998]. The winter season was chosen to minimize the effects of

transpiration of water by deep-rooted plants [*Scholl et al.,* 1998]. The potentiometric surface indicated that the hydraulic gradient was approximately 2.8 m/km north of the Norman Landfill and 1.4 m/km south of the landfill. It also showed that the direction of the groundwater flow was generally north-northeast to south-southwest, toward the Canadian River.

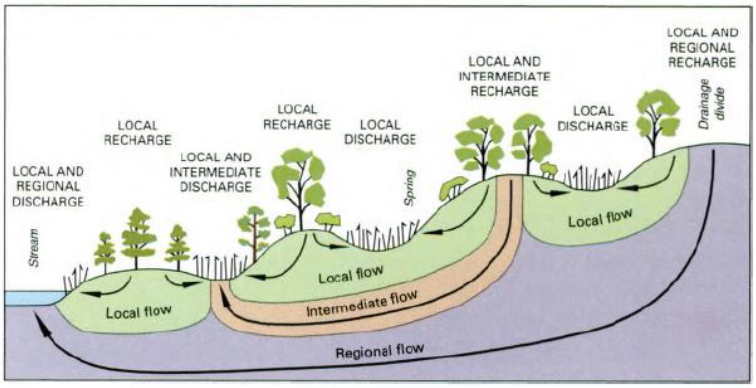

Figure 3. Ground water flow system: Local, intermediate and regional ground water flow systems related to topographic highs and lows. Source:[*Carter,* 1996; *Winter,* 1976]

2.1.6. Canadian River

The Canadian River is a low-sinuosity sand-bed river, which changes in pattern from braiding to meandering [*Marston et al.,* 2001]. Natural migration or flood activity of the stream inundates the floodplain without barrier until the edge of the landfill [*Marston et al.,* 2001]. The Canadian River floodplain sediments include sand bars and mud layers. The geomorphology of the river is a consequence of the continuous dissection of the sand bars formed by braiding of the channel and mud layers developed as silt and clay settles from suspension each time [*Marston et al.,* 2001].

2.1.7. Topography

The highest elevation of the domain is found on the west cell reaching 343 m while the lowest points are near the wetland and the Canadian River. The landfill accepted municipal solid waste from the early 1920's and then in the 1960's and 1970's waste was buried in shallow trenches and covered with sand [*Christenson et al.,* 2003]. By the time the landfill was closed, the fills were covered with earthen caps. The capped landfills rise 12-13 m above the floodplain [*Christenson et al.,* 1999].

2.2. Methods and Data

Groundwater models are computer programs of groundwater flow systems for the analysis of groundwater flux and their interactions with the atmosphere and surface water [*Todd et al.*, 2005]. The uncertainty exists in the configuration of the physical system, including the values of its parameters, input variables and field observations, plays a large role in the nature of a groundwater system. Also because of the simplifying assumptions embedded in the mathematical equations, a model must be viewed as an approximation and not an exact representation of a real world system. The key to proper conceptualization of a system is to avoid oversimplification or under-simplification [*Todd et al.*, 2005]. With an oversimplified conceptual model we cannot capture the essential features of the system which leads to a numerical model that is powerless of simulating observed field conditions. In contrast, an under-simplified conceptual model tends to make the numerical model too complex and computationally demanding. [*Todd et al.*, 2005]

2.2.1. Model Development

Development of the groundwater flow model involved the following steps: (a) collecting and analyzing data, (b) developing the conceptual model and mathematically simulating it, (c) calibrating the model for the year 1998-1999, (d) and validating for the year 2005. Recent developments of numerical methods for approximations of the groundwater-surface water flow system make it convenient to simulate complex hydrology systems [*Winter,* 1976]. MODFLOW-2000 was used to construct the local scale transient model by numerically solving the two-dimensional groundwater flow equation for a porous medium.

A number of software packages were used to facilitate the groundwater investigation in the study area. A geographic Information Systems (GIS) tools allowed organizing a considerable quantity of groundwater and surface water information in addition to expediting analysis through their ability to manage and map the data. Visual MODFLOW v.2010 [*Schlumberger Water Services et al.*, 2010] provided a graphical-user interface for preparing MODFLOW-2000 inputs and for viewing model outputs. It was used to input GIS files, visualize the input data, run MODFLOW-2000 and display the results. The PEST [*Doherty,* 2004] tool was used to estimate the parameters of interest. PEST is a nonlinear model-independent parameter estimator equipped with an inversion engine and the ability to set bounds on parameters while minimizing the discrepancy between model results and field observations. The Marquardt-Lavenberg algorithm [*Gill et al.*, 1978; *Press et al.*, 1992] implemented in PEST has to minimize the weighted sum of squared differences between model-generated observation values

and those actually measured in the field. HYDRUS-1D [*Simunek et al.,* 1998] which is a modeling environment for variably saturated porous media was used for calculations of potential evapotranspiration.

Based on the complexity of the domain and data availability, a 2-D approach was preferred over 3-D simulation. By choosing the *x*- axis along transect A-A' while the *z*-axis is aligned in the direction of gravity, the flow variations in the *y*-direction were ignored. The *y*-axis runs approximately parallel to the span of the wetland. The 2-D model is by integrating the 3-D form of the Darcy equation coupled with the continuity equation over the length of the wetland. Development of Equation (2.1) is discussed in most textbooks of groundwater hydrology [*Domenico,* 1972; *Todd et al.,* 2005].

$$\int_{l_1}^{l_2} \frac{\partial}{\partial x}(K_{xx}\frac{\partial h}{\partial x})dy + \int_{l_1}^{l_2} \frac{\partial}{\partial y}(K_{yy}\frac{\partial h}{\partial y})dy + \int_{l_1}^{l_2} \frac{\partial}{\partial z}(K_{zz}\frac{\partial h}{\partial z})dy - \int_{l_1}^{l_2} W dy = \int_{l_1}^{l_2} S_s \frac{\partial h}{\partial t} dy \qquad (2.1)$$

K_{xx}, K_{yy}, and K_{zz} are the hydraulic conductivities along the *x*,*y* and *z* coordinates, respectively, *h* is the potentiometric head, *W* is the volumetric flux per unit volume representing sinks or sources. S_s is the specific storage of the porous medium and *t* is time. K_{xx}, K_{yy}, K_{zz} and S_s are functions of space (*x*,*y*,*z*) and *W* is a function of space and time (*x*,*y*,*z*,*t*) [*Todd et al.,* 2005]. The interval of the integration [l_1, l_2] is roughly the distance across the wetland. The integration leads to the following form:

$$\frac{\partial}{\partial x}(K_{xx}\frac{\partial h}{\partial x})(l_2 - l_1) + \frac{\partial}{\partial z}(K_{zz}\frac{\partial h}{\partial z})(l_2 - l_1) - W(l_2 - l_1) = S_s(l_2 - l_1) \qquad (2.2)$$

by adopting two simplifying assumptions:

1) $\frac{\partial h}{\partial y} = 0$ which means that the pressure head of the wetland does not change significantly with respect to *y* (along the length of the wetland). In other words, it indicates that the potentiometric gradient in the *y*-direction does not change. This is a reasonable assumption for a vegetated wetland since the vegetation reduces the flow and decreases the velocity of water [*Carter*, 1996].

2) *W* and S_s do not change in the y-direction, showing that there is no considerable sink or source affecting the water flow in *y*-direction . The storativity and time variability of the pressure head are also negligible in this direction.

The length of the wetland (l_2-l_1) cancels out on both sides of Equation (2.2); therefore, the governing equation is independent of the *y* dimension. In order to get the actual fluxes throughout the slough extent, the solution of the model must be multiplied by (l_2-l_1).

It is true that the above-mentioned simplifying assumptions of the 2-D approach could be a source of uncertainty in the water balance calculations but the lack of sufficient data creates a bottleneck for building a 3-D groundwater flow model. Notwithstanding, the 2-D framework may lead to a perception of the nature of stream flow dynamics in the Norman Landfill site, which can then be expanded into a more complicated 3-D simulation when the physical processes are relatively well-understood.

The 2-D finite difference model consists of 1 row, 37 columns, and 9 layers. Totally, 333 grid cells cover the profile area of about 52,380 m^2. The resolution of grids near the wetland was made finer to adjust for the greater flow concentration and larger

number of field observations of hydrologic conditions. Geometry of the layers refers to the horizontal geologic units described by *Scholl et al.* [1998] and *Marston et al.* [2001]. The transient model simulates groundwater flow using daily time step. MODFLOW-2000 has a series of modules for various types of boundary conditions. In addition to the Basic (BAS) module that provides the overall program control and Layer-Property Flow (LPF) module, the following head-dependent and head-independent modules were chosen to construct the model.

2.2.1.1. River Module

The effect of flow between the Canadian River and groundwater system were modeled via a seepage layer separating the surface water body from the groundwater system using the River module. Depending on the hydraulic gradient between the river and the groundwater system, the river may either contribute water to the groundwater system, or act as a groundwater discharge zone. The underlying assumption in this approach is that leakage through the river bed does not change the river stage [*McDonald et al.*, 1998].

2.2.1.2. Lake Module

The head-dependent Lake module developed by *Merrit et al.*[2000] was used to simulate the wetland. The implicit assumption of this module is that the variation of the wetland stage is in response to the hydraulic stresses applied on the aquifer and the other external stresses. The wetland is represented as a finite volume of space within the model. The Lake module relies on an independent water budget that accounts for the

seepage, rainfall, overland runoff, evaporation and anthropogenic gains and losses. The riparian area of the wetland allows a funnel effect that concentrates runoff towards the wetland. This means that the rate of precipitation would need to be increased proportionally to encompass the rate that runoff entering the wetland.

Estimation of the daily evaporation rate of the wetland for the years 1998-1999 were obtained by using linear regression analysis of the 2005 pan evaporation data. The dependent variables were precipitation, relative humidity, air temperature, wind speed and solar radiation. Transpiration rates of the phreatophyte type of vegetation calculated by the Penman-Monteith equation were also taken into account.

2.2.1.3. ET Module

A third head-dependent package is the Evapotranspiration Segments (ETS1) module developed for use with MODFLOW-2000 by [*Banta,* 2000]. It evaluates the water loss in the water budget from plant ET at the ground surface by removing water from the saturated groundwater regime. When the water table is at or above the elevation of the top grid cell, ET loss occurs at a maximum rate. When the water table exceeds a specified depth known as the “extinction depth”, ET rate is zero. Between these two limits, the rate of the ET varies based on the defined relation between the ET rate and hydraulic head. The relation adopted decreased the ET rate monotonically with increasing slope toward the extinction depth. This approach to calculate the actual ET is not precise in the sense that ET losses from the unsaturated zone are not taken into account. More accurate estimations of ET and vegetation habitat modeling require extensive information about the ecosystem of the Norman Landfill site including crop

growth data and root water uptake parameters. Lack of these information restricts using more advanced packages for MODFLOW-2000 such as RIP GIS-NET [*Ajami et al.*, 2012] and HYDRUS [*Twarakavi et al.*, 2008]. The landfill modeling domain was divided into six zones to account for the different vegetation types that exist there, and their ET rates and extinction depths. Four zones were assigned to the topographic prominences of the mound area. The wetland bank has its own ET zone, and the rest of the domain up to the Canadian River was allocated as the sixth ET zone.

2.2.1.4. Well Module

Regional groundwater recharge was simulated using the well module; therefore, the recharge rates were calculated based on the potentiometric map of the site. Regional groundwater flow in the winter season runs toward the Canadian River with the hydraulic gradient approximately 1.4 to 2.2 m/km. The average groundwater velocity based on this hydraulic gradient, the median hydraulic conductivity from slug tests (6.6×10^{-5} m/s) and median porosity of 0.34 was found to be about 2.71×10^{-7} to 4.27×10^{-7} m/s. The respective pumping rates calculated according to the continuity equation were about 5.2 to 8.3 m^3/day for winter time, and lower during the summer season. Seasonal variation for the pumping rate was considered during the calibration to honor the seasonal pattern of the regional groundwater recharge.

2.2.1.5. Recharge Module

Surficially distributed recharge to the groundwater system was simulated by assigning recharge boundary condition to the top grid cells of the model. Recharge rate

is a pre-requisite for efficient groundwater simulation and it was assumed to be a percentage of the precipitation. The multiplier depends on many factors including land use and vegetation type, surface topography, soil cover material and antecedent soil moisture condition [*Eagleson,* 1978; *Todd et al.,* 2005]. A comprehensive recharge process at the site was studied by *Scholl et al.* [2006] through analysis of stable isotopes and water table fluctuations. Their findings from recharge, ET and seasonal groundwater observation analyses point out that the infiltration rate is greatly affected by the ET rate during the growing season. The plant roots easily uptake the needed water from percolating rainfall in both saturated and variably saturated zones during the growing season. Therefore, a substantial amount of percolating water is removed by the vegetation before reaching the water table. During the dormant season the net recharge rate is significant and ET rate is insignificant. The opposite occurs in the growing season. The possible reasons behind these characteristics of the recharge process are: (a) the densely vegetated site during the growing season increases the interception which reduces the deep infiltration, and (b) more rain events happen in winter time when there is no demand for ET. Part of this water moves downward by gravity into the saturated zone and in the meantime fills the pores in the unsaturated zone up to the specific retention. Since there are very limited ET losses in the root zone, the soil reaches saturation by the late winter. This situation clearly describes the antecedent soil moisture condition at the beginning of the growing season. The recharge boundary condition was distributed on the domain in five recharge zones. The area on the landfill mound with its steep topographic terrain and grass-type vegetation differs in infiltration

rate with the riparian zone of the wetland with gentle topography and shoreline plants. zone 1 was assigned to the mound area, and zone 2 to the distance between the toe of the landfill and left bank of the wetland. The area between the right bank and the Canadian River is zone 3, the right bank is zone 4 and the left bank was assigned zone 5 .

2.2.1.6. Time Domain

In both calibration and validation simulations, the time series graph of the water level for the wetland is about 0.8 m below the water level in well WLMLF. Additionally the fluctuations in the wetland showed more dynamic behavior than the water level in the mound (Figure 4).

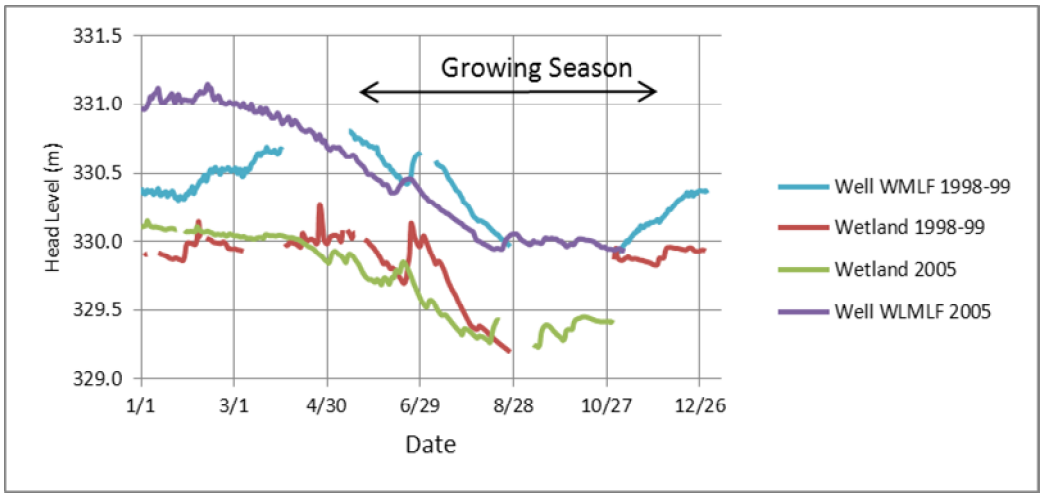

Figure 4. Time series of the measured water levels in wetland and well WLMLF during the year 1999 and 2005. Growing season starts about mid-April through October.

The calibration study was conducted from November 1st, 1998 until August 8th, 1999, encompassing 298 transient stress periods. Validation study was carried out from January 1st, 2005 to November 8th, 2005. Although the water fluctuations in well

WLMLF showed very fast response time (hourly) (Figure 5), the forcings driving the hydrological cycle such as precipitation and solar radiation have daily measurements that put limitation to the length of the stress periods. This limitation enforced the hydrological processes in the model to operate in daily stress period.

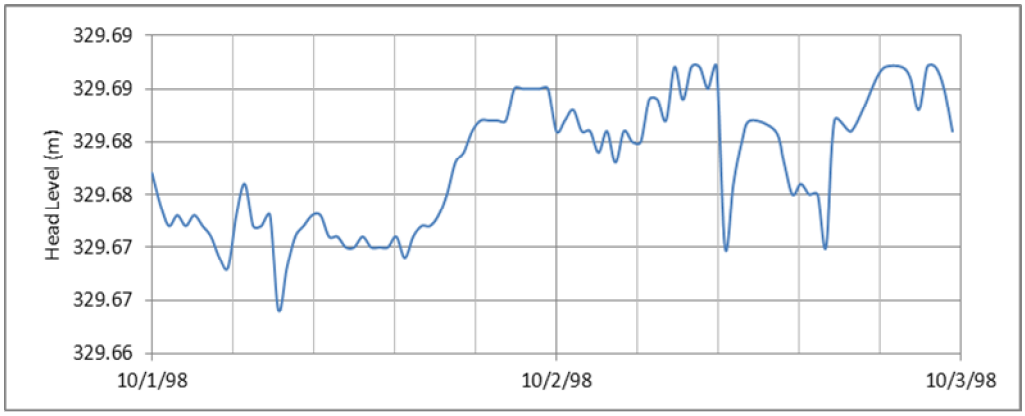

Figure 5. Water level measurements in well WLMLF in period of 48 hours.

2.2.2. Meteorological Data

Meteorological data including historical daily precipitation, average relative humidity, air temperature (maximum, minimum, and average), wind speed, mean sea level pressure and total solar radiation were obtained from the Norman station of the Oklahoma MESONET [*www.mesonet.com*, 1994]. Local measurements of precipitation, wind speed, relative humidity and solar radiation were also obtained from the USGS Norman Landfill Project [*http://ok.water.usgs.gov/projects/norlan/*] . Sunshine hours as well as geographical parameters were acquired from the National Weather Service [*NWS Internet Services Team*]. The Moderate Resolution Imaging Spectroradiometer (MODIS)

provides spectral details important to modeling of the Earth's energy budget. The level-4 MODIS global Leaf Area Index (LAI) product which is available every 8 days at 1 km resolution was retrieved from the MODIS website [*http://modis.gsfc.nasa.gov*]. This quantity expressed as the area of leaf per area of ground and it is unit less [*Jordan,* 1969]. The LAI values for both riparian area and landfill mound were 10 to 14 during the summer and gradually decreased to 1 to 3 in the winter. Evaporation data for the wetland were obtained from measurements made by [*Masoner et al.,* 2008] using a modified Class A floating evaporation pan for the period of February through August 2005.

2.2.3. Hydrological Data

Measurements of the stage of the Canadian River and the wetland were collected from the USGS gaging station 07229050 (Canadian River at Norman, Latitude 35°11'40", Longitude 97°29'05") and gaging station 07229053 (Canadian River Tributary at Norman, Latitude 35°10'02", Longitude 97°26'53"). The data set includes daily values for mean discharge, gauge height and water stage. Groundwater level measurements in the three wells alongside transect A-A' and continuous surface-water measurements in the wetland were obtained from the USGS Toxic Substances Hydrology Program-Norman Landfill Project [*http://ok.water.usgs.gov/projects/norlan/*].

This program provides data sets containing the raster data of the digital elevation model (DEM), vector data sets including hydrography of the domain, bathymetry of the wetland, potentiometric surface, delineation of the landfill cells, and water levels. A

groundwater level monitoring well (WLMLF) was drilled through the west cell of the landfill and continuously measured the groundwater level at 30 minute intervals with an accuracy of 3.5 cm [*Becker*, 2002]. The other two groundwater monitoring wells (Well IC 36 and Well IC 54) had sparse as monthly data sets.

2.2.4. Geological Data

Besides the head monitoring wells, 5 slug test wells used to characterize hydraulic conductivity variations in the domain were situated near transect A-A'. The unconfined alluvial aquifer at the site is 10 to 15 m thick, composed of unconsolidated sedimentary deposits ranging from clay to gravel with medium grained sands being dominant [*Scholl et al.*, 1999] (Figure 6). The aquifer is underlain by Hennessey Shale which acts as a confining unit [*Scholl et al.*, 1998]. The altitude of the bedrock was obtained from *Becker* [2002] and it was measured using shallow seismic shear-wave refraction data and drilling information.

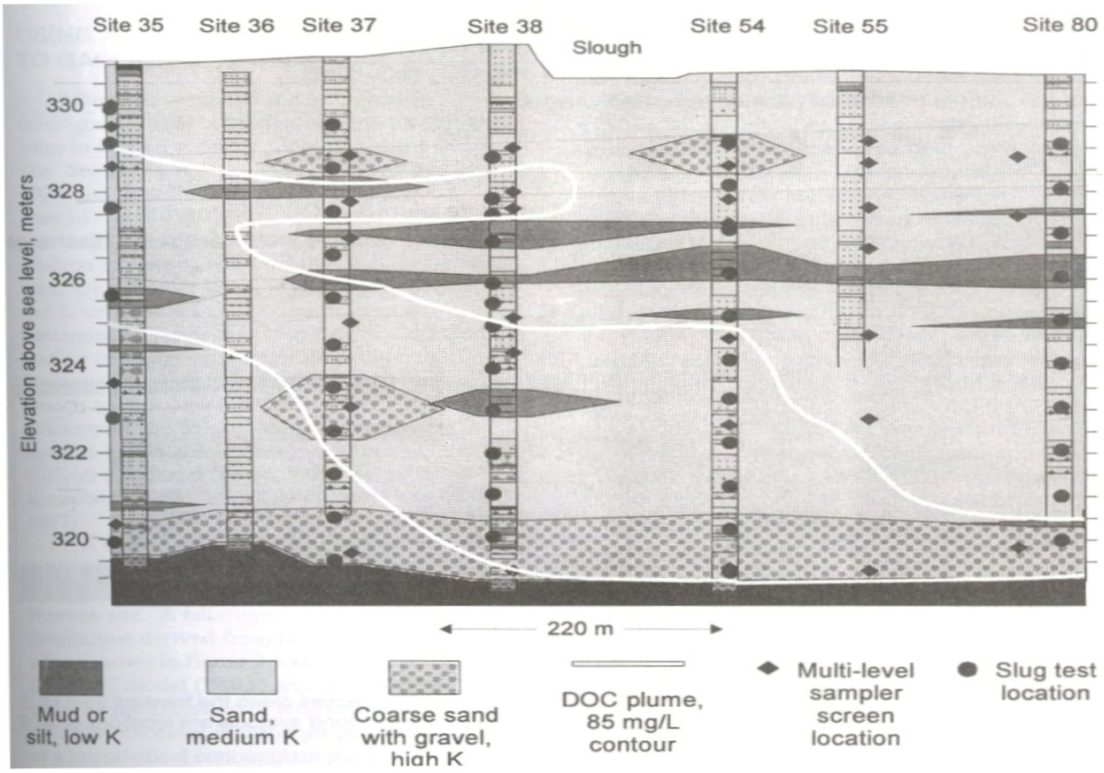

Figure 6. Permeability structure of the alluvium plain along transect A-A' at the Norman Landfill site using core description and slug test results (Source : [*Scholl et al.*, 1999])

The Canadian River alluvium aquifer consists of fluvial sediments of the Canadian River. According to the laboratory tests and core analyses reported by USGS, porosity ranged from 0.34 to 0.44 for the alluvium aquifer [*Scholl et al.*, 1998]. This range expands from 0.40 to 0.92 for the material of the landfill mound. Specific yield (S_y) is defined as the volume of water that an unconfined aquifer releases from storage per unit surface area per unit decline in the water table [*Todd et al.*, 2005]. This parameter is unit less and varies with the grain size distribution of the aquifer material and the height of the water table, the capillary fringe above the water table, the depth of the water table below the land surface, the magnitude of the change in water level,

whether the water table is rising or falling, and the time allowed for the aquifer to reach equilibrium [*Nachabe*, 2002]. At the Norman site, water table rise followed rain events within 24 hours [*Scholl et al.*, 1999] . For this short term fluctuations of the water table, a range of 0.10-0.30 for the alluvium aquifer and even less for the landfill mound were considered part of the initial data [*Scholl et al.*, 2006; *Todd et al.*, 2005]. S_y varies based on hydraulic conductivity and hydrogeological situation and in this study six S_y zones were utilized (Figure 7).

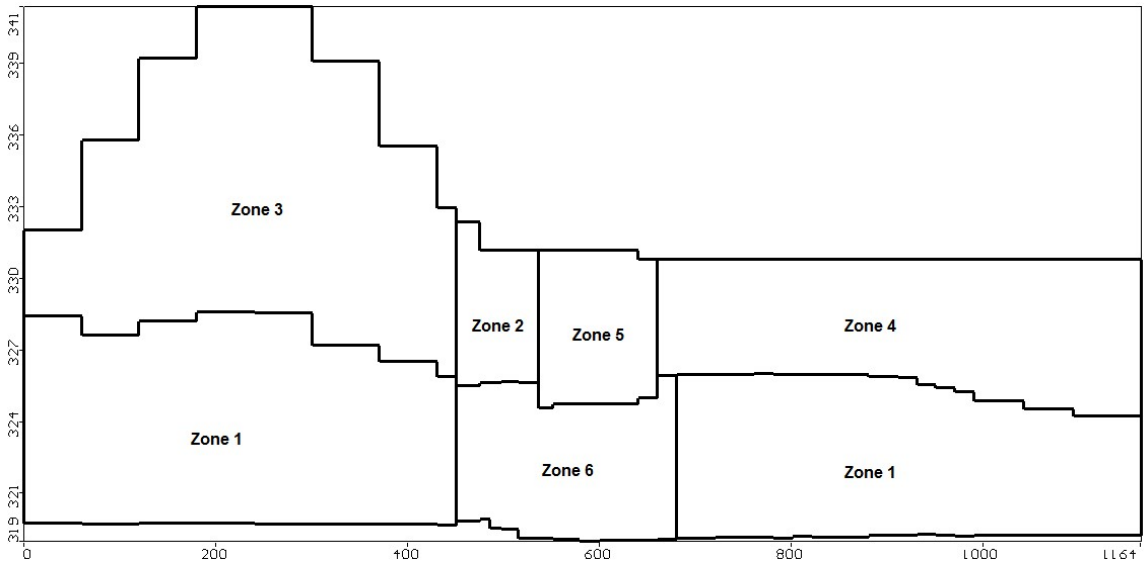

Figure 7. S_y is allocated into six zones. Zone 1 contains the lower layers except the Slough area. The upper layers are divided into 4 zones: the mound area, the area between the mound and riparian, the riparian and the area between the riparian and Canadian River

Martson et al. [2001] used conductivity logs and soil cores, and *Scholl et al.* [1998] used slug tests to verify the existence of a high permeability coarse gravel layer in the alluvium aquifer located at the base of the alluvial fill. This layer acts as a

preferred permeability pathway within 1.5 m above the lower confining unit. The stratigraphy of the floodplain described by *Martson et al.* [2001] and *Scholl et al.* [1998] defined the geometry and thickness of the alluvium layers. The former study demonstrated that the alluvium was partitioned into five layers.

- A basal layer consisting of coarse grained sediments and gravel with thickness ranging from 1.8 to 2.4 m from base of the alluvium.
- Sand layers about 3 m thick overlying the basal layer.
- A layer ranging in thickness from 4.5 to 6.0 m, characterized by extensive mud layers and clay lenses above the sand layer.
- Another sand layer overlying the mud layers with 2.4 to 2.7m of thickness.
- The top layer extending 1 m down from the ground surface composed of very fine-grained sands.

This classification of the aquifer layers depicted the stratigraphic heterogeneity of subsurface sediments and the variability pattern of hydraulic conductivities was assigned accordingly (Figure 8). A study of spatial variation of hydraulic conductivity using the slug test reported a wide range of 8.4×10^{7} to 2.8×10^{-4} m/s with a median value of 6.6×10^{-5} m/s [*Scholl et al.*, 1998].

The least known attribute needed in mapping the physical heterogeneity of the soil is the ratio of the horizontal to the vertical hydraulic conductivity (K_x/K_z). This ratio is important particularly in areas of recharge and discharge where the wetland interacts with groundwater [*Winter*, 1976]. *Winter* [1976] discussed the importance of this ratio and concluded that if the ratio were to be less than 100, surface water is rarely lost to the

groundwater system. If the ratio was greater than 1000, surface water is lost under many conditions, and a ratio between 100 and 1000 indicates other controlling factors to become dominant in the interaction of the surface water and groundwater systems. Considering the *Winter* [1976] study, ratios of 300, 500 and 700 were tested for the geologic matrices around the wetland.

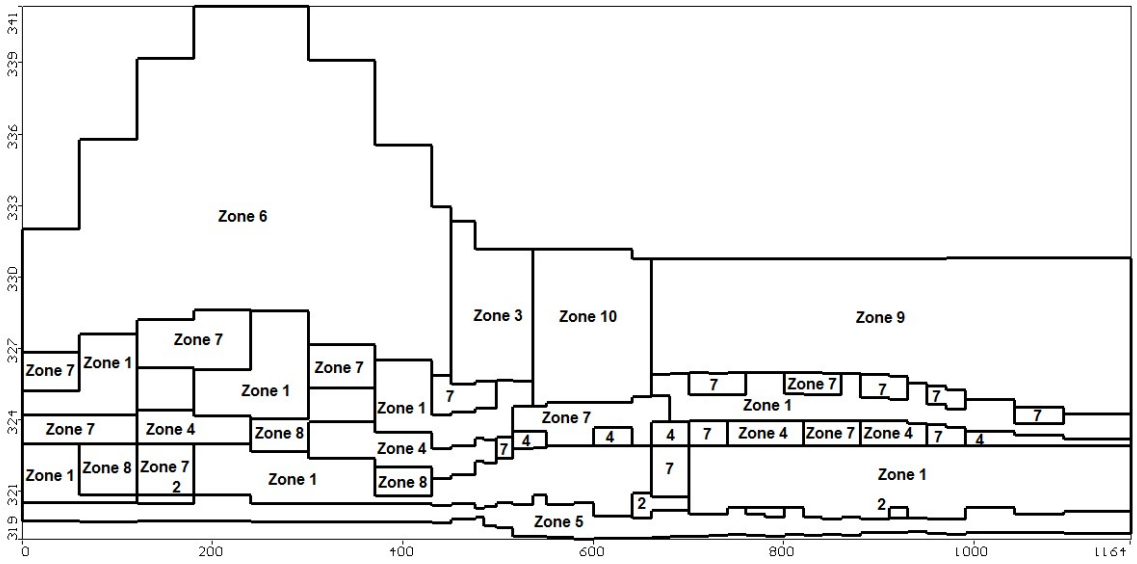

Figure 8. Hydraulic conductivity zones assigned for study area at the Norman landfill site. Totally 10 zones were allocated to represent the heterogeneity in the domain.

2.3. Results and Discussion

The model proposed in this study was able to adequately describe the fundamental hydrological processes and useful to understand the contributions of different processes to the overall water balance. It also showed the relative importance of each component of water balance varies both spatially and temporally. However it is worth to note that there is no fully objective model as a result of uncertainties in

conceptualizing the aquifer layers and stratification, boundary conditions, parameter distributions and dominant stresses. There could be alternative plausible conceptual models, yet using the same original information but in a different manner.

The time series discrepancy of the water balance for the validation simulation represents the temporal changes in the flow mass balance which means the difference between the total flow IN and total flow OUT expressed as a percentage of the total flow (Figure 9). The discrepancy percentage varied in range of ±4% with the maximum discrepancy between the simulation and observation data appearing on January 7th , 2005.

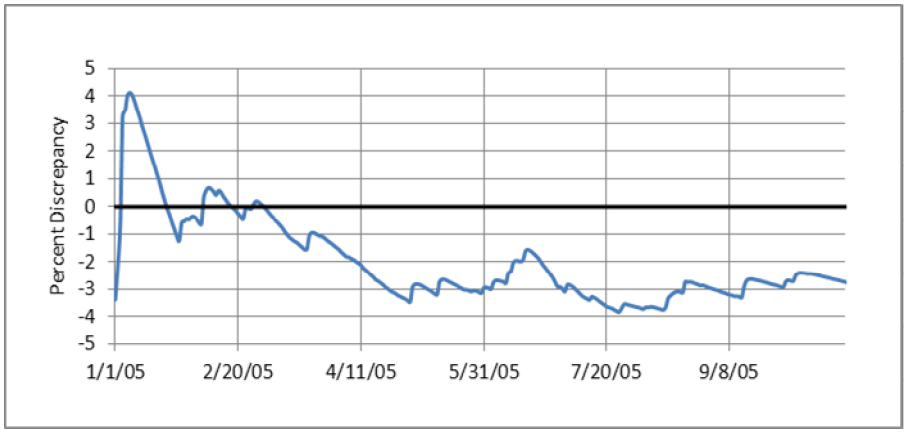

Figure 9. Percent discrepancy graph plots the temporal changes in the flow mass balance (total flow IN – total flow OUT) expressed as percentage of the total flow for the validation simulation.

2.3.1. Calibration Results

The process of model calibration was done by applying both PEST and trial-and-error parameter adjustment .The goodness-of-fit of the calibrated model was basically based on a visual judgment by comparing the observed and the simulated pressure heads and the numerical measures of the goodness-of-fit such as the normalized root mean squared error (NRMS) between the observed and simulated pressure head and the correlation coefficient. Indeed there is no generally accepted objective measure of comparison and the judgment is subjective [*Madsen*, 2000]. As a consequence the NRMS of 15%, correlation coefficient of 0.85 and confidence interval of 90% were adopted to assess explicitly the soundness of the model. The calibration results of the model in terms of pressure head for four observation locations with overlying precipitation rates are shown in Figure 10 and the statistical details are given in Table 1.

The 1:1 scatter plot of calculated vs. observed pressure head values for the year 1998-1999 is presented in Figure 11. The plot shows the comparison between the values calculated by the model (x- axis) and the values measured in the wells (y-axis). If all the data points intersect the 45 degree bisector line ($x=y$) on the graph, then it characterizes a perfect calibration scenario which is not likely to happen for real situations. Points that appear above the bisector line denote positive residuals indicating the model is over predicting and points appearing below the bisector line represent negative residuals indicating that the model is under-predicting the pressure head. The 95% confidence intervals are also shown in Figure 11 which allows visualization of the range of

calculated values within the 95% intervals. The graph shows that the majority of the data points laid in the acceptable confidence intervals.

A

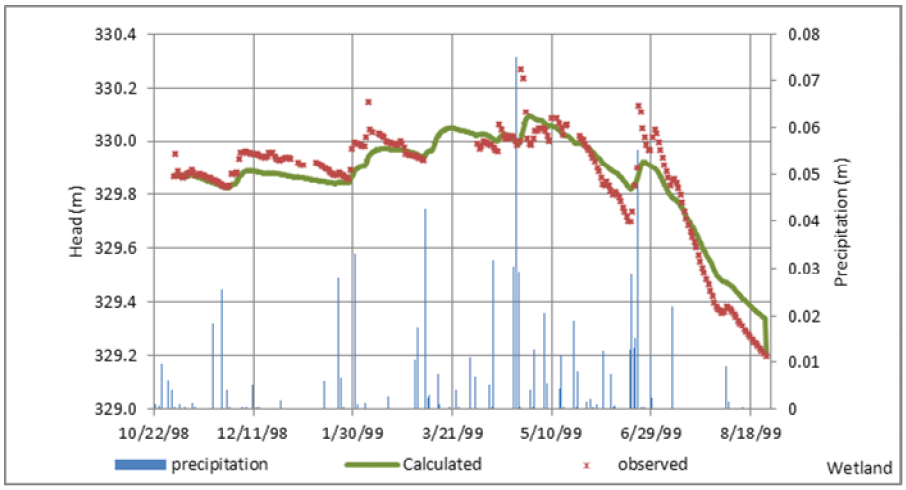

B

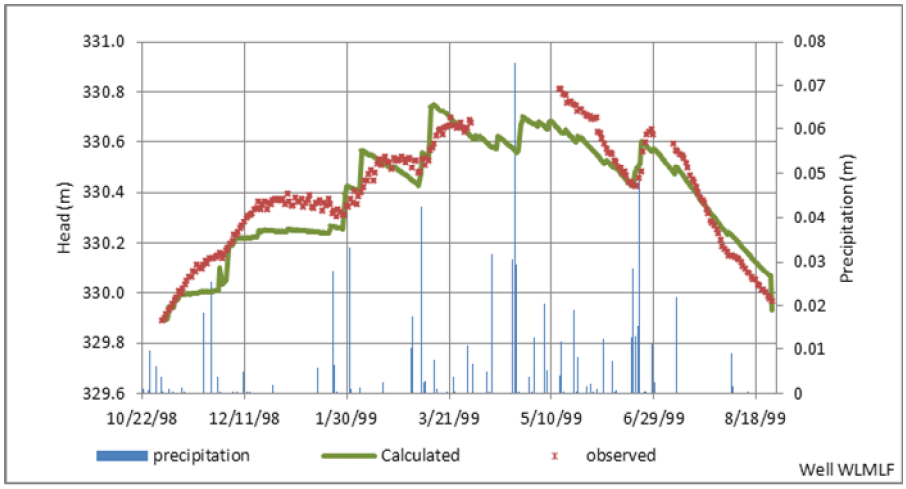

Figure 10. Calibration graphs of the calculated and observed pressure head at the Norman site for the four observation points (A) Wetland , (B) WLMLF, (C) IC 54 and (D) IC 36

C

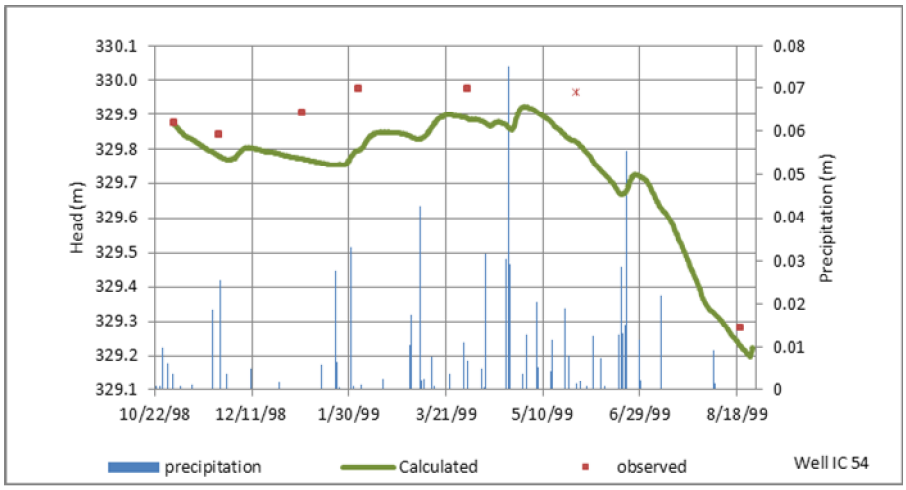

D

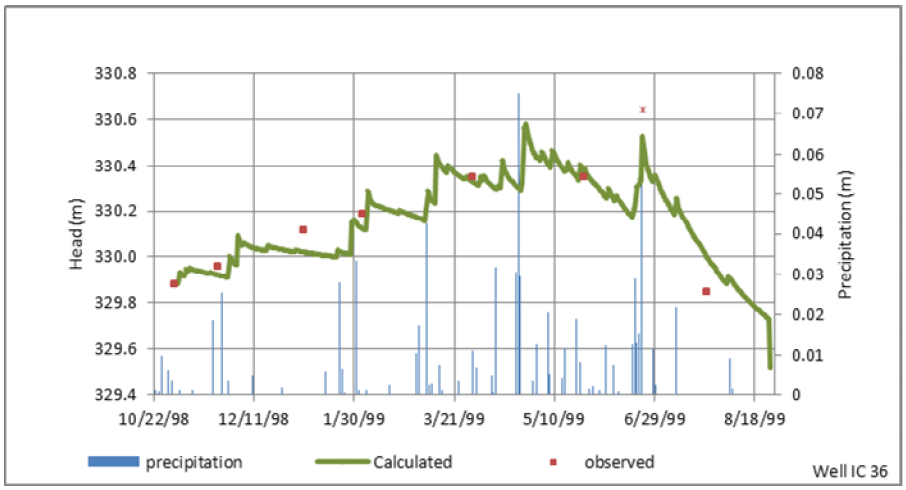

Figure 10. Continued.

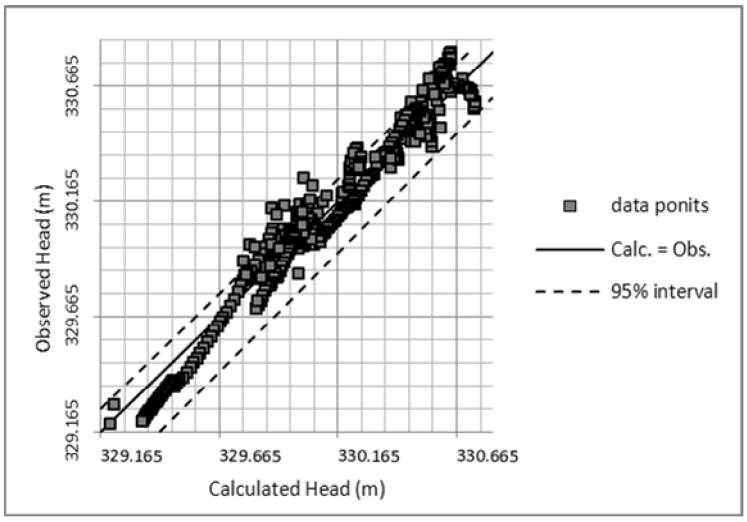

Figure 11. Scatter graph of the calculated vs. observed pressure head values for the calibration simulation and overall statistical results.

Table 1. Statistical results for the calibration simulation. NRMS stands for normalized root mean squared error and Res. stands for residual

Well	NRMSE	Correlation Coefficient	Max Res. (m)	Min Res. (m)	Mean Res. (m)
WLMLF	9.74	0.97	-0.18	0.00	0.07
SLOUGH	6.86	0.95	-0.27	0.00	-0.01
IC 36	10.77	0.87	-0.42	0.00	-0.02
IC 54	14.84	0.96	-0.20	0.00	-0.08
Overall	6.845	0.96	-0.42	0.00	-0.03

2.3.2. Validation Results

The results of the validation study for the year 2005 are shown in Figure 12 and the statistical details are given in Table 2. Data was available only from the wetland and well WLMLF during this period. Figure 13 represents the 1:1 scatter plot of calculated vs. observed pressure heads for the validation study. It is seen that the majority of the data points are in the 95% confidence intervals. Histograms of the distribution of residuals for the wetland, well WLMLF and all data points together are shown in Figure

14. Ideally the distribution of the residuals for a large number of data points is clustered around the value of zero and resembles the Student distribution curve. The Student distribution curve which was obtained by normalizing residual values was also displayed to determine the likelihood of calculated data points. Figure 14 showed that although the residual histogram for the wetland and well WLMLF did not exactly follow a normal distribution, the residual histogram of the all data points together did follow a normal distribution.

Apart from statistical point of view, the calibration and validation simulations shared the following hydrological characteristics. Both the calibration and validation graphs showed that the high level phase of pressure head started from the beginning of the first autumn/winter rain event and lasted to mid- June and the low level phase lasted from mid-June through September (Figure 10 and Figure 12). Although the water table rise and fall are in phase with the timing of recharge events, the distinct seasonal patterns also induced the hydrologic regime of the groundwater system. In other words, the groundwater net recharge is tightly linked to precipitation and ET; therefore the water table fluctuates with dry and wet cycles as well as seasonally. The diurnal water table fluctuations in the wetland demonstrated that there is a functional association between water stage and riparian phreatophyte transpiration. The long-term climatic cycle and the Canadian River stage also influence the wetland stage in a longer time scale.

A

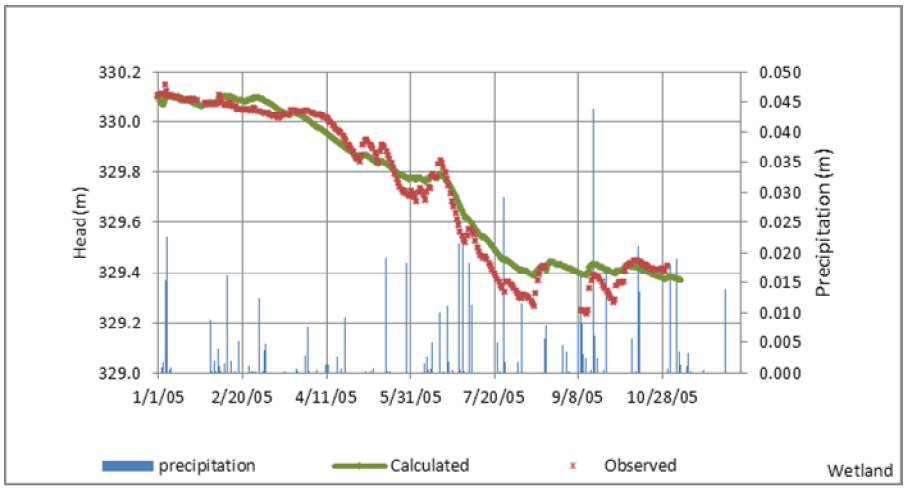

B

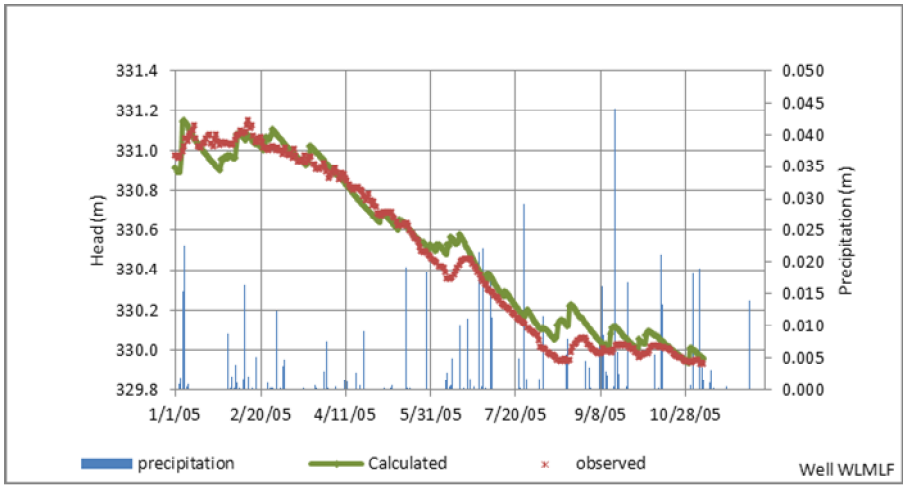

Figure 12. Validation graphs of the calculated and observed pressure head at the Norman site for the (A) wetland and (B) WLMLF

Table 2. Statistical results for the validation simulation. NRMS stands for Normalized Root mean Squared and Res. stands for Residual

Well	NRMSE	Correlation Coefficient	Max Res. (m)	Min Res. (m)	Mean Res. (m)
WLMLF	6.53	0.99	0.66	0.00	0.05
Wetland	6.14	0.99	0.27	0.00	0.03
Overall	4.27	0.99	0.32	0.00	0.04

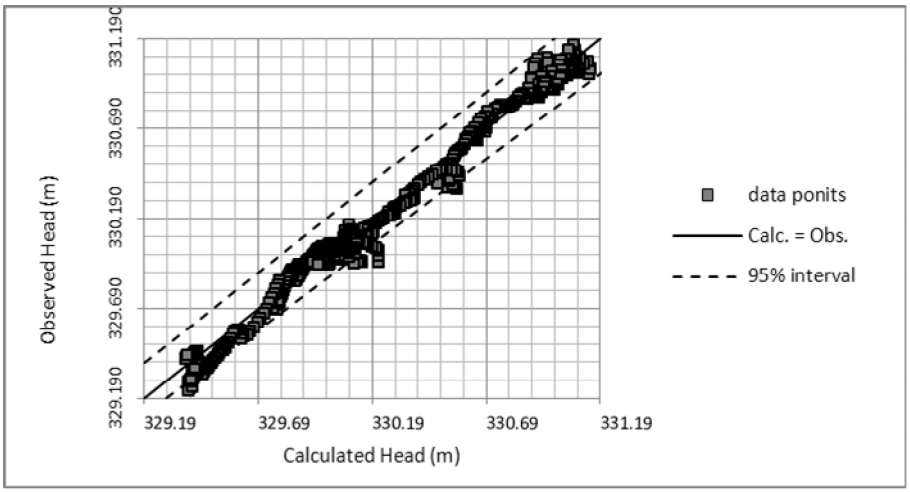

Figure 13. Scatter graph of the calculated vs. observed pressure head values for the validation simulation and overall statistical results.

A

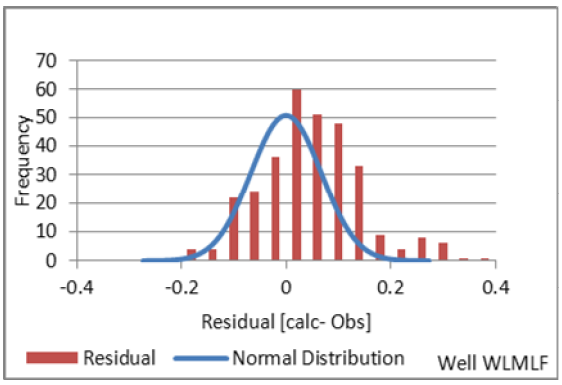

B

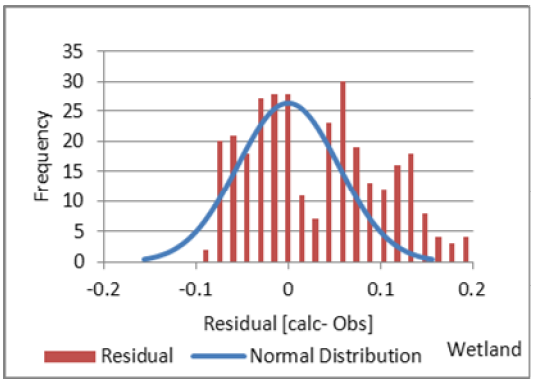

Figure 14 . Residual histogram of the (A)WLMLF , (B) wetland and (C) overal points of the validation simulation

C 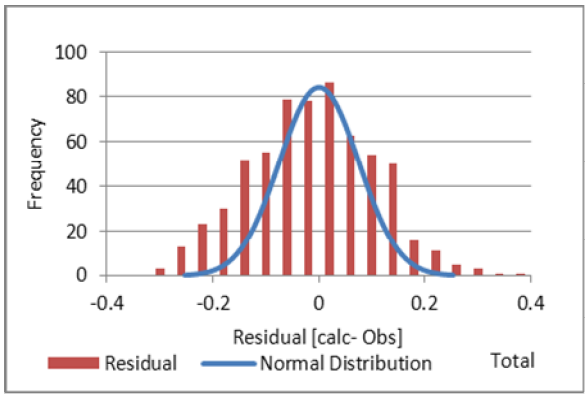

Figure 14. Continued.

2.3.3. Hydraulic Conductivity

Horizontal hydraulic conductivities estimated from PEST were in agreement with the permeability structure suggested for the domain by *Marston* [2001] (Figure 15). Cells bordering the wetland had K_x/K_z ratios of approximately 1000. The hydraulic conductivities that were assigned to the geologic matrix were representative of sand, gravel, clay, silt, loam and peat. Sensitivity analyses for the hydraulic conductivity showed that the model was primarily sensitive to the horizontal hydraulic conductivity of the highly permeable bottom layer (zone 5) and secondly to the K_x of zone 1. K_x of the zone 7 as well as both K_x and K_z of the mound area (zone 6) and K_z of the zone 1 also showed relatively large sensitivity values. The uncertainty analysis for hydraulic conductivities implied that the K_x of zone 5 has the highest uncertainty .

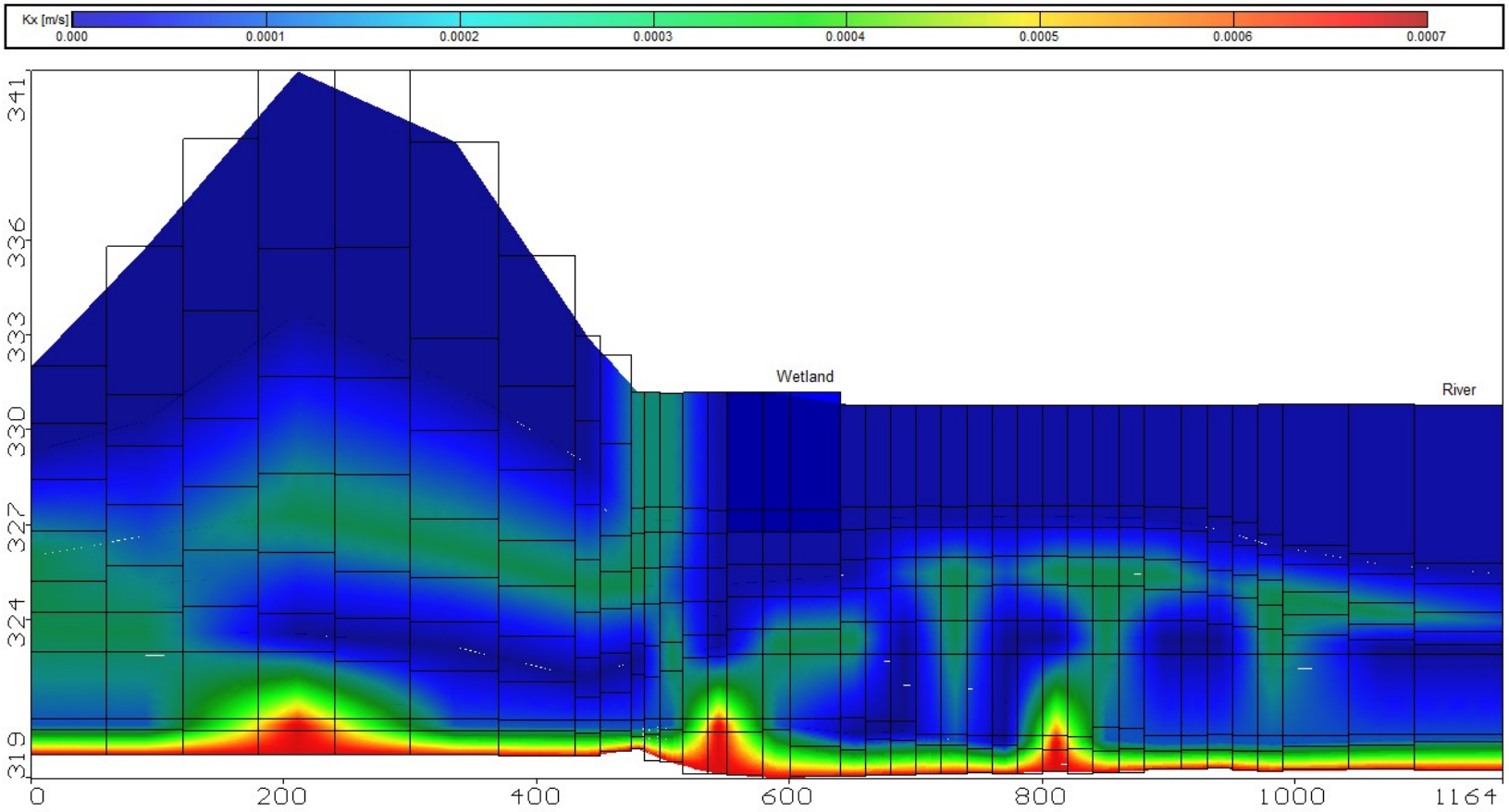

Figure 15. Horizontal hydraulic conductivity distribution in cross section

2.3.4. Specific Yield

Variability of the specific yield (S_y) in the Norman Landfill is significant and analyses showed that even the top layer of the transect did not have a unique value which can be interpreted as significant heterogeneity of the top layer soil. The S_y for the landfill mound and riparian area were estimated to be 0.08 and 0.17, respectively, while for the rest of the top layer grid cells S_y was estimated to be 0.19. The estimated S_y in the lower layers was 0.18 (Figure 16). Sensitivity analyses results showed that the S_y values controlled the amplitudes of the fluctuations in the water table at well WLMLF (Figure 17). Higher values of the S_y had a damping effect and lower values increased the amplitude. The variability in the S_y parameters of each zone is shown in Figure 18.

2.3.5. Recharge Parameters

Table 3 shows the values of the recharge multiplier for both the growing and dormant seasons. The wetland receives direct precipitation and some runoff from the surrounding uplands. The zones 2, 4 and 5 representing the riparian area of the wetland, have the greatest recharge multipliers for both seasons. The large difference in recharge rates between the riparian area and other zones can be explained by considering the topography and landscape. The ground slope causes the excess precipitation that falls outside the wetland to be transported in the direction of the wetland. The vegetative composition and soil type of the wetland bank reduce the water flow velocity and the water has a chance for deep percolation into the ground. A significant seasonal difference in recharge multiplier appearing in zone 1 (landfill mound) can be related to

the substantial difference of the vegetation during the actively growing or dormant seasons.

Table 3. Recharge Multiplier values for different zones and different seasons in the Norman Landfill site

Zone	1	2	3	4	5
Growing Season	0.23	0.7	0.34	0.7	0.45
Dormant season	0.69	0.8	0.35	0.80	0.54

2.3.6. Head Equipotential Map and Water Flow Velocity Vectors

The results of the numerical simulation of the Norman Landfill in terms of head equipotential values, velocity vectors and water table levels for the first day of months January and July 2005 are shown in Figure 19 to represent the winter and summer time. The velocity vectors in the bottom layer clearly show the pathway for subsurface water flow, which is towards the Canadian River. The water table in the wetland is at its maximum level in January and gradually declining with time to reach its minimum in August. The velocity vectors in the direction of wetland point out that the seepage occurred mainly into the wetland. The velocity vectors under the mound showed significant velocities (indicated by the length of the arrow) in summer time although the recharge multipliers for the mound area during the growing season are relatively small in comparison to the dormant season. These high infiltration rates may relate to the low wetting front and more intense rain events during the growing season. The velocity fields of groundwater flow in the two different seasons also represent the direction and magnitude of the regional, intermediate and local groundwater flow in the domain across time.

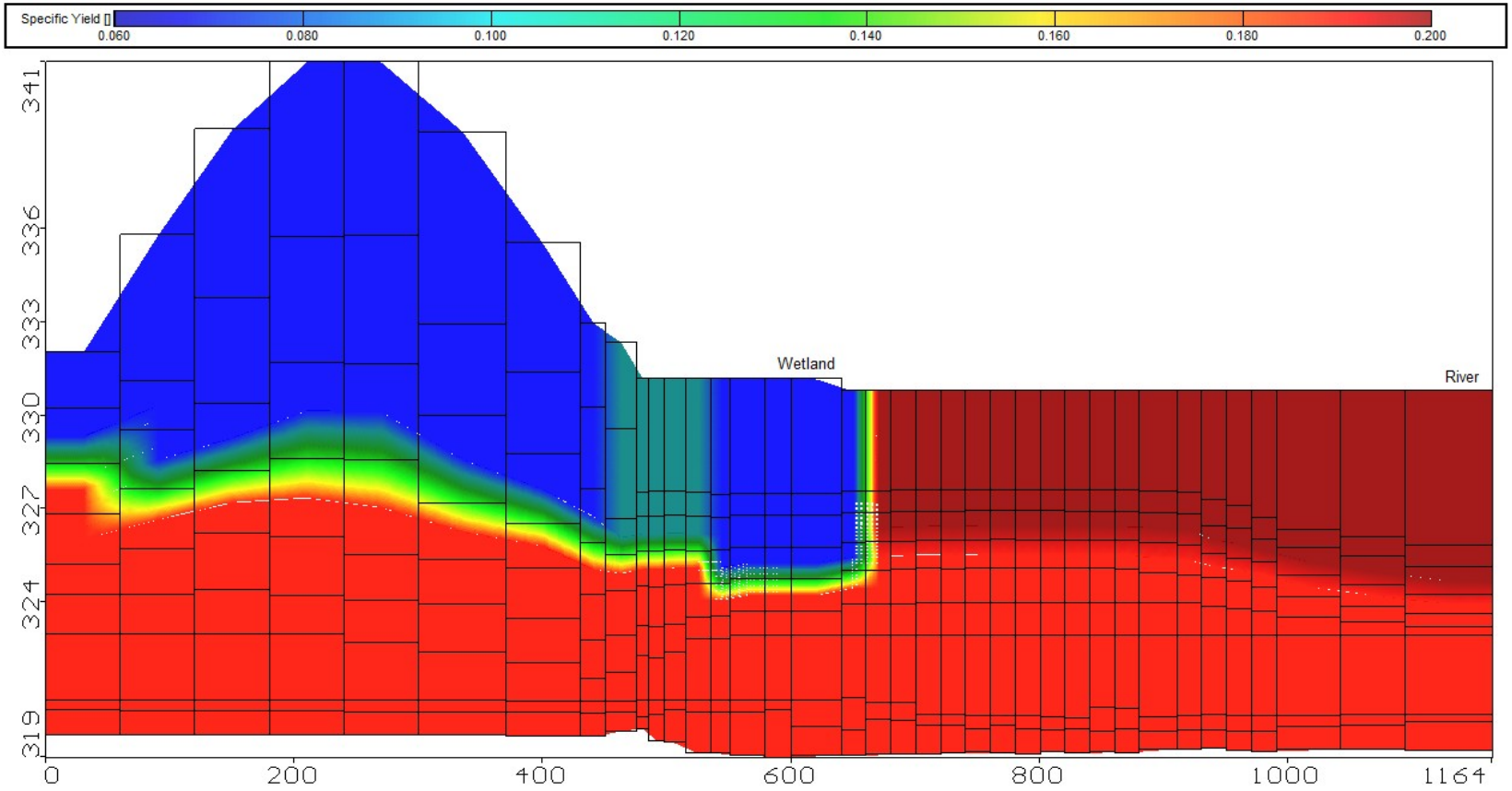

Figure 16. Spatial distribution of specific yield in cross section

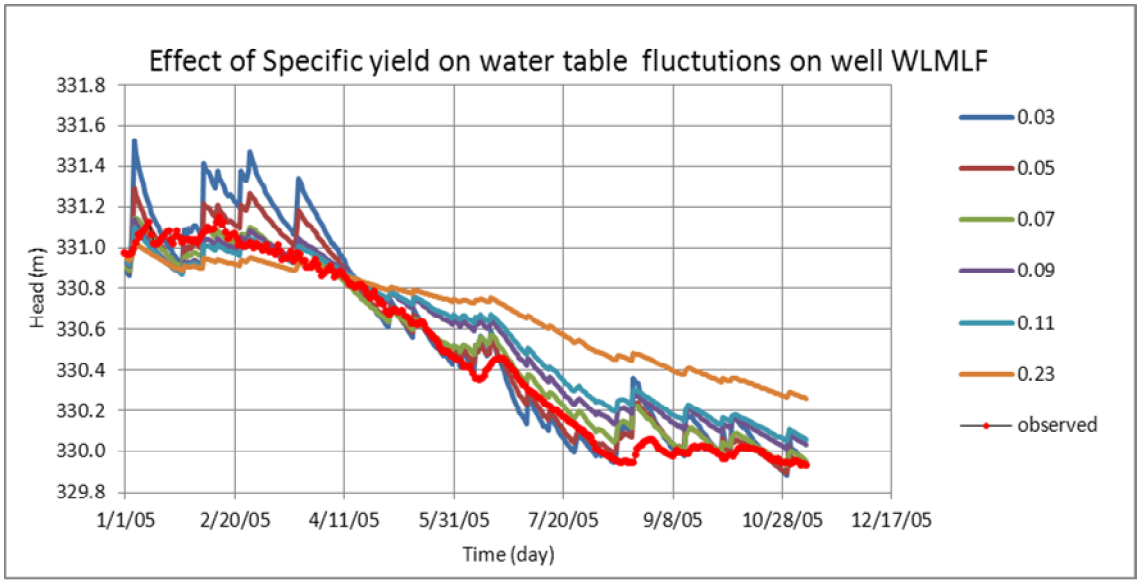

Figure 17. Sensitivity of the water level in the well WLMLF with respect to specific yield value of the mound area (zone 3)

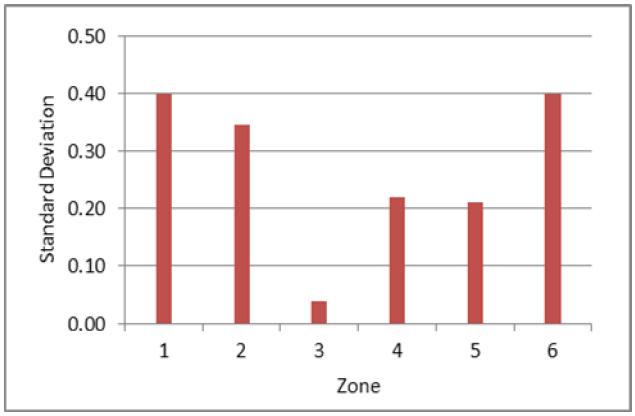

Figure 18. Uncertainties associated with specific yield parameters

A

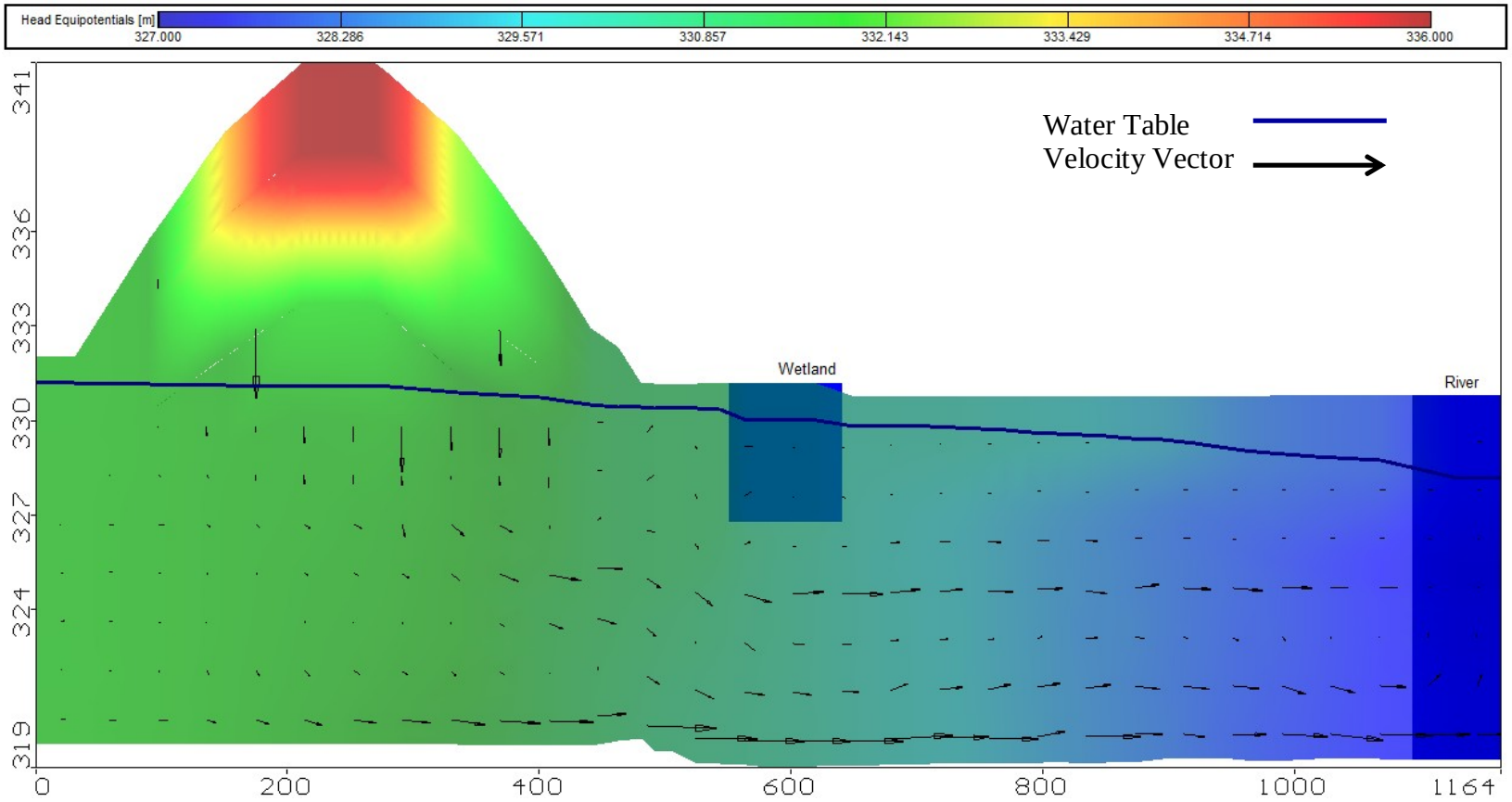

Figure 19. Head equipotential map, velocity vectors and water table elevation in cross section of the Norman landfill site. (A) January 1st and (B) July 1st, 2005

B

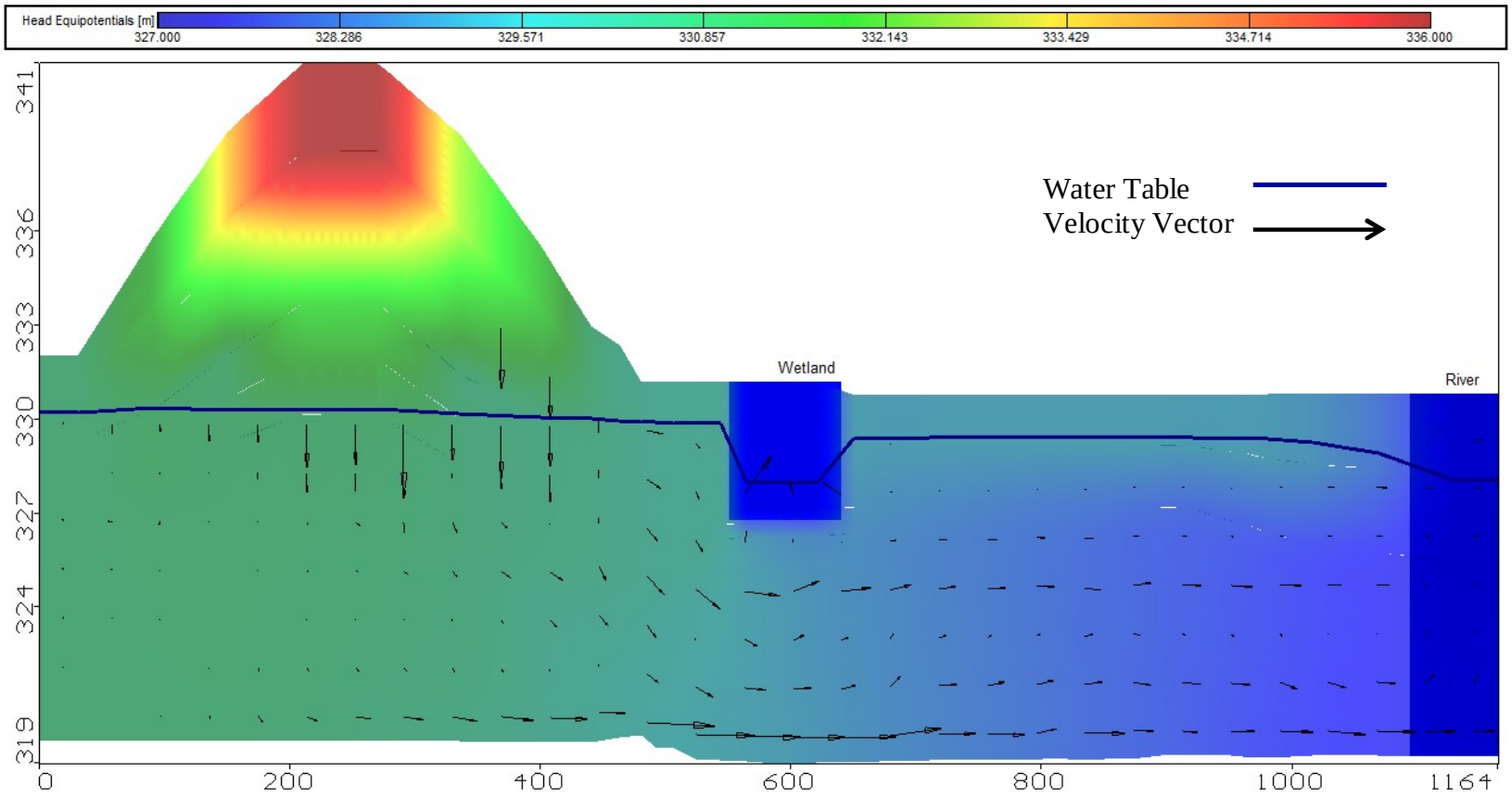

Figure 19. Continued.

2.3.7. Water Balance Components

2.3.7.1. Aquifer Storage

Time series plots of the temporal changes in the rate of aquifer storage are shown in Figure 20. STORAGE IN is the rate of mass added to the system through sources (precipitation, regional groundwater recharge) and STORAGE OUT is the rate of reduction in mass storage. The STORAGE IN peaks in June and July and STORAGE OUT peaks in September and May. Storage capacity is lowest during the dormant season when plants are not transpiring heavily and the wetland stage is high. During the growing season, storage capacity increases as ET increases and wetland stage decreases.

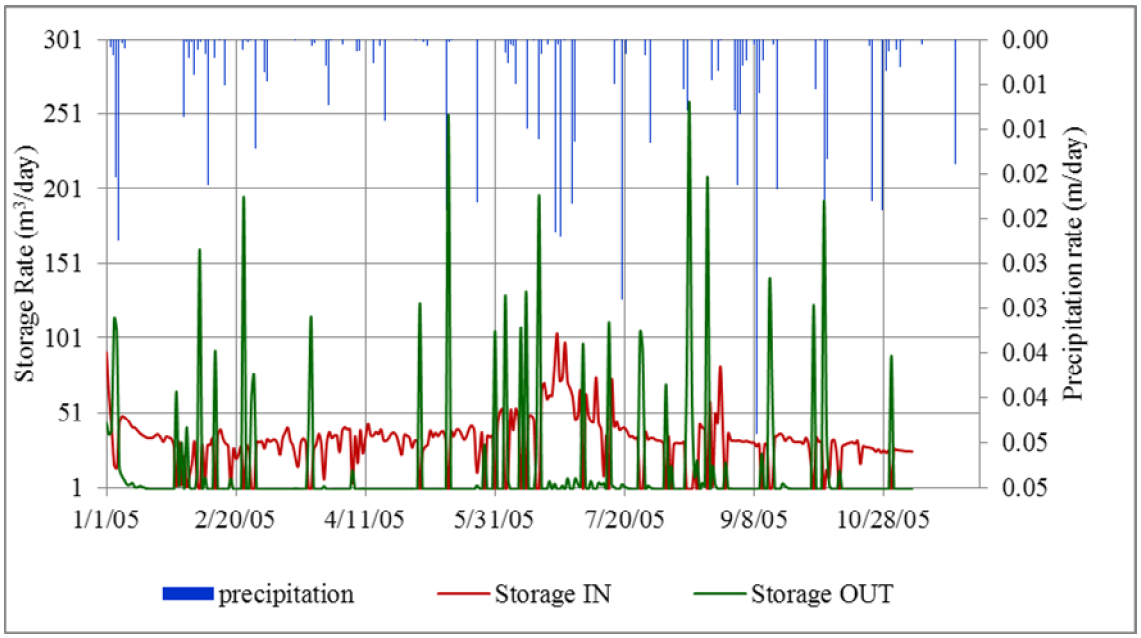

Figure 20. Aquifer storage rate IN and OUT from the system for the validation simulation . (m^3/day)

2.3.7.2. Wetland Seepage

Groundwater discharge occurs through ET when the plant roots reach the water table and through seepage when the water table in the wetland or river is lower than the groundwater in aquifer bordering the wetland or river. The wetland stage is approximately 0.8 m below the local groundwater level, which means that generally seepage occurs from the surficial aquifer to the wetland and the result of the simulation recognized the flow-through the wetland process (Figure 21). Flow reversal may also occur when groundwater flow direction from the riparian area to the wetland shifts back to the riparian area during the active growing season mainly because of high ET rates from phreatophyte vegetation [*Doss*, 1993]. Usually this reversal occurs at a very small scale in the vicinity of the wetland and thus the model could not completely capture this hydraulic gradient between the water level in the riparian zone and the wetland.

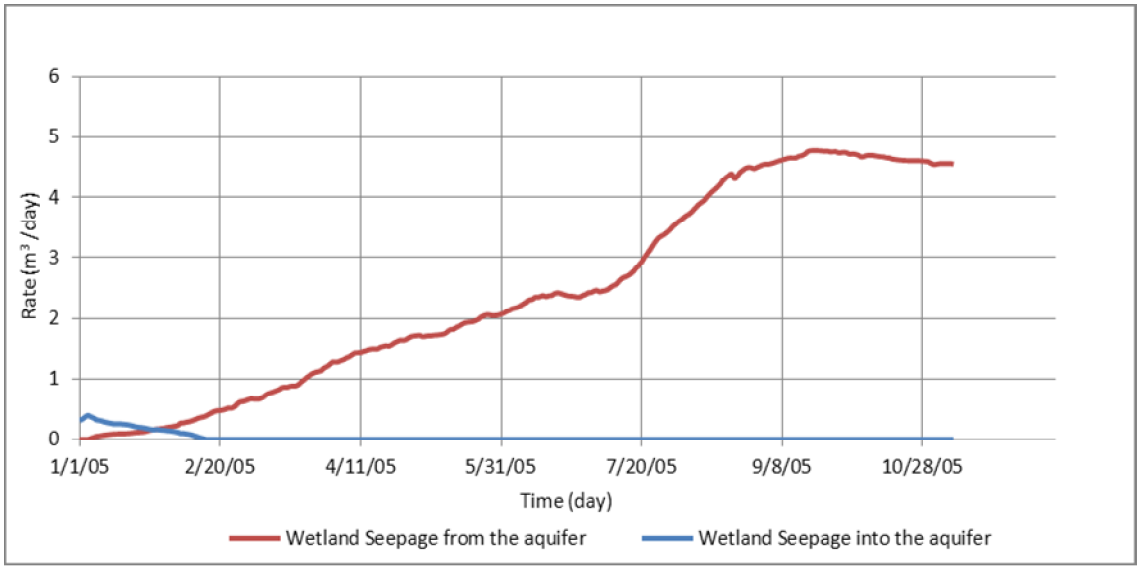

Figure 21. The wetland seepage rate into and from the aquifer (m^3/day).

2.3.7.3. River Leakage

Leakage into the Canadian River is shown in Figure 22 with rather decreasing pattern in winter time and fairly consistent leakage rate during the growing season. The Canadian River always acts as a sink for the groundwater and its water stage variability affects the leakage rate.

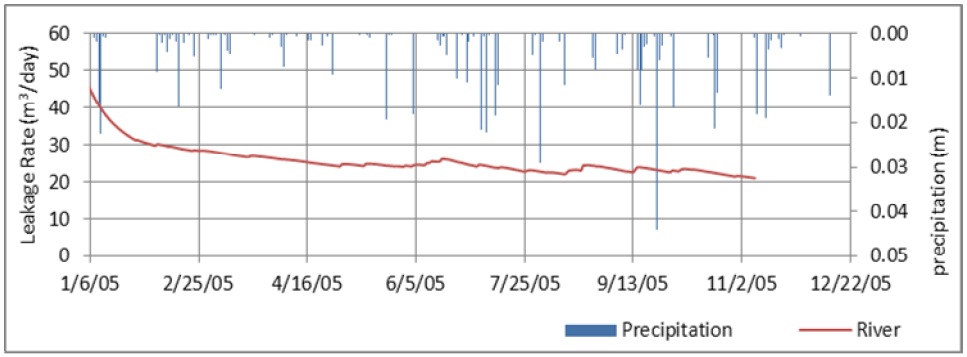

Figure 22. Leakage rate into the Canadian River for the validation simulation (m^3/day)

2.3.7.4. ET

Loss of water to the atmosphere is a key component in the water budget of the Norman Landfill. ET rates are highly variable seasonally, daily and spatially [*Carter*, 1996]. ET losses from the landfill vary with plant types, density and status and also water table elevation. During the active growing season in May, ET rate starts increasing gradually (Figure 23) and in June and July, ET rates are at the highest levels. The ET gradually decreasing through October and in the winter, it is at its minimum rate. ET rates were plotted for four zones in the domain: wetland, mound, riparian and the area between the right wetland banks to the Canadian River (Figure 24). ET in the mound

was found to have a different pattern in that it reached its peak rate about twenty days earlier than the other zones. Possible reasons for this phenomenon in the growing season could be shallow rooted vegetation on the landfill mound. In the riparian area the water table was shallow and water availability and soil moisture was not a limiting factor for the ET. Thus the controlling factors are status of the riparian plants and climatological condition. Analysis showed that the ET rate in the wetland calculated by the model was higher than the floating pan evaporation measurements (Figure 25). Apart from the uncertainty existing in the model and measurements, this comparison implied a high rate of phreatophyte transpiration in the wetland.

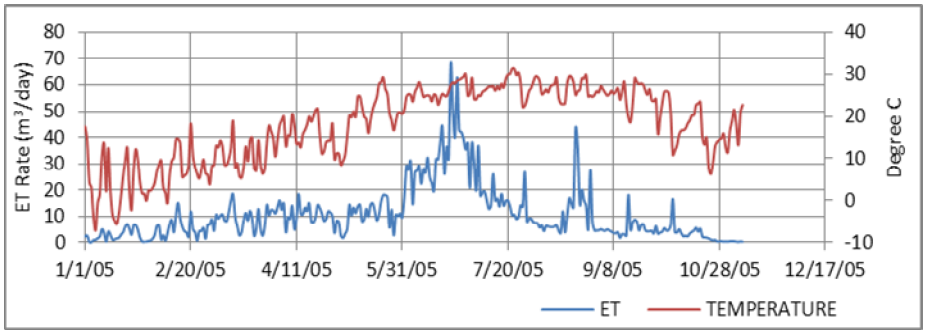

Figure 23. Total ET from the domain for the validation simulation (m^3/day)

A

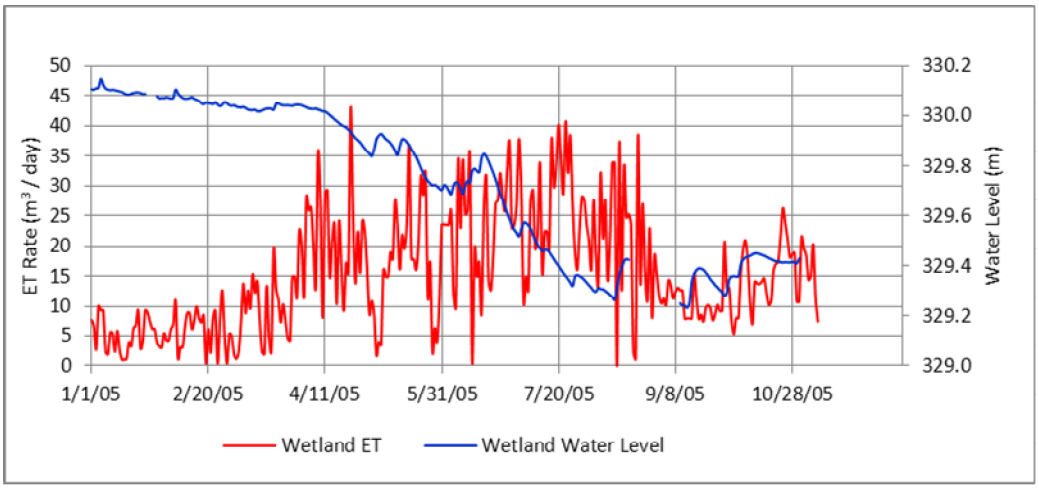

B

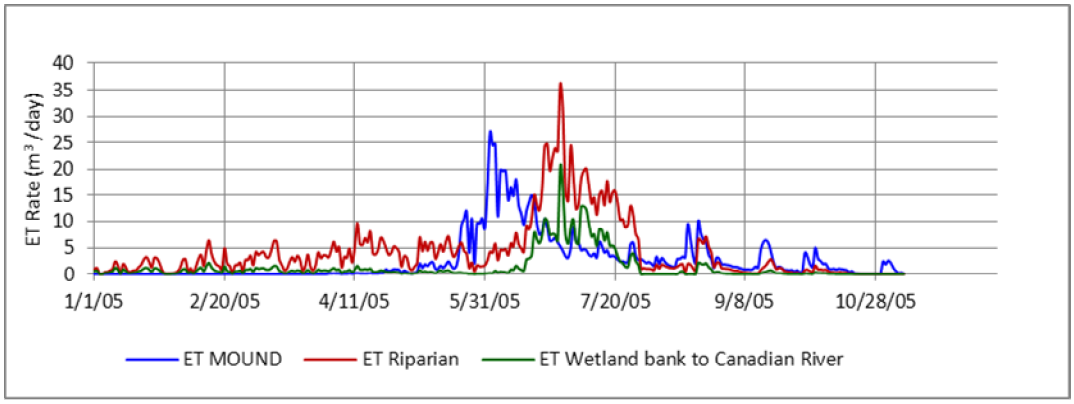

Figure 24. (A)ET rate for the wetland for the validation simulation which has negative correlation with the wetland stage. During winter time, the wetland stage is high and the ET rate is low and during the summer time, the wetland stage decreased while the ET rate increased .(B) ET rate by zones for the validation simulation (m^3/day). Mound ET is in different phase with the wetland and riparian ET

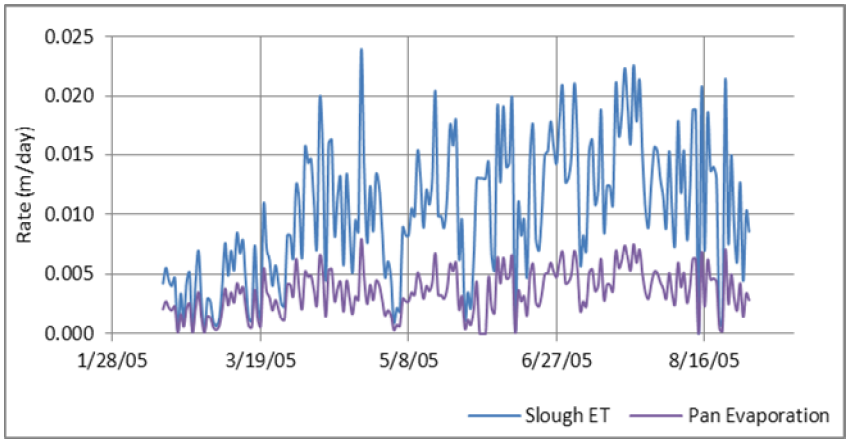

Figure 25. Calculated wetland ET and pan evaporation measurement for the year 2005. The difference indicates the rate of transpiration in the wetland.

3. A MARKOV CHAIN MONTE CARLO METHOD FOR THE GROUNDWATER INVERSE PROBLEM

A MCMC method for the groundwater inverse problem is presented in this section. The model was tested for a hypothetical 2-D saturated flow in a heterogeneous porous medium .

3.1. Statement of the Problem

The 2-D transient groundwater flow in a saturated heterogeneous porous medium, satisfying both the continuity equation and Darcy's law and subject to initial and boundary conditions was solved using MODFLOW-2000. The partial-differential equation of groundwater flow used in MODFLOW-2000 is:

$$\frac{\partial}{\partial x}(K_{xx}\frac{\partial h}{\partial x})+\frac{\partial}{\partial z}(K_{zz}\frac{\partial h}{\partial z})+W=S_s\frac{\partial h}{\partial t} \tag{3.1}$$

Here K_{xx} and K_{zz} are values of saturated hydraulic conductivity along the x and z coordinate axes (L/T); h is the potentiometric head (L), W is a volumetric flux per unit volume representing sources and/or sinks of water (T^{-1}), S_s is the specific storage of the porous media (L^{-1}). The anisotropy ratio for K_{xx}/K_{zz} was considered 10 and throughout the study, the unknown parameter K_{xx} was referred to as K_s. In this study, we treated $Y(u)=ln\,[K_s(u)]$ as a random function with mean $\langle Y(u)\rangle$ and covariance function $C_Y(u)$ in which $u=(x,z)$ is the vector of the two Cartesian coordinates. We assumed that there were n_Y measurements of $Y(u)$ and n_h measurements of hydraulic head at one observation location (n_h different times). Then the problem was to determine the $Y(u)$ by combining

Bayesian updating of $Y(u)$ given the natural log (K) measurements $Y_0 = \{Y(u_1),...,Y(u_n)\}^T$ and hydraulic head measurements $h_0 = \{h_1,...h_n\}^T$.

3.2. Representation of the Parameters

MODFLOW-2000 solves Equation (3.1) using the finite-difference (FD) method in which the groundwater flow system is divided into a grid of cells and for each cell, there is a single node at which hydraulic head is calculated [*Harbaugh et al.*, 2000]. The number of the parameters in $Y(u)$ field was considered to be equal to the number of nodes (m) in the discretization of the groundwater flow system. In general the number of parameters being estimated is much larger than the number of measurements and the inverse problem may become ill-posed [*Hadamard*, 1902]. Therefore a compromise must be made by reducing the number of parameters to be estimated without losing the ability to reproduce spatial variability [*Carrera et al.*, 2005].

3.3. Bayesian Inference

3.3.1. Statistical Model and Likelihood Function

The Metropolis algorithm [*Metropolis et al.*, 1953] was implemented as a generic method of approximation to the posterior pdf corresponding to any combination of prior pdf and likelihood function. The likelihood function was defined using a forward model (G) , known model parameters (d) , unknown model parameters $Y(u)$ and observed data (h_0). In this study, the forward model was MODFLOW-2000 and the known model parameters (d) included all the required parameters of the forward model subject to the

appropriate boundary conditions, excluding $Y(u)$. The measurement error ε was represented by the following model:

$$h_i = G[d_i, Y(u)] + \varepsilon_i \qquad i=1,\ldots,n \tag{3.2}$$

where ε_i was assumed to be an independent and identically distributed (i.i.d.) random variable from a normal distribution with a mean of zero and a unconditional variance of $\sigma^2 = 1.0$.

The model provided a complete specification of the joint probability density of the observed data, $h_1,\ldots h_n$, conditional upon the data and the model parameters [d , $Y(u)$] [*Hoff*, 2009]. In this manner, the combination of the forward modeling and measurement errors were assumed Gaussian which allowed the likelihood function to be characterized by the normal pdf [*Hoff*, 2009; *Woodbury et al.*, 2000] where:

$$\begin{aligned} & p(h_1,\ldots,h_n \mid G[d,Y(u)],\sigma^2) \\ & = \prod_{i=1}^{n} p(h_i \mid G[d_i,Y(u)],\sigma^2) \\ & = (2\pi\sigma^2)^{-\frac{n}{2}} \exp\{-\frac{1}{2\sigma^2}\sum_{i=1}^{n}(h_i - G[d_i,Y(u)]^2\} \end{aligned} \tag{3.3}$$

3.3.2. Prior Information

Bayesian statistical inference also required a prior pdf $\pi(Y)$ for the parameters $Y=(Y_1,\ldots,Y_m)^T$ which represented our judgment about the Y(u) field. In practical data analysis situations, it is hard to mathematically formulate our prior beliefs and thus $\pi(Y)$ is often chosen in a somewhat ad hoc manner or for reasons of computational

convenience [*Hoff*, 2009]. Still, specifying a prior pdf for the model parameters in a logical and consistent way is a fundamental problem [*Woodbury et al.*, 2000].

Geostatistics is generally considered to be a reasonable choice for the estimation of the appropriate prior pdfs for hydrogeological applications [*Chen et al.*, 2001; *Copty et al.*, 1995; *Deutsch et al.*, 1998; *Ezzedine et al.*, 1999; *Journel*, 1989]. The 2-point statistics-based simulation is a geostatistical means for generating multiple equiprobable realizations of the random variable which aims at reproducing a covariance or variogram model. A variogram model is a statistical relation between any two values $Y(u)$ and $Y(u+l)$ in space in which l denotes a lag vector representing separation between two spatial locations [*Remy et al.*, 2008] . A variogram model indicates how the various constitutive random variables relate to each other and to the data ($Y_0(u)$). The 2-point simulation generates L number of equally probable realizations using the sequential Markov Chain process.

The Sequential Gaussian Simulation (SGSIM) algorithm [*Journel*, 1993] was utilized in this study to get the prior pdf for the model parameters. In the SGSIM algorithm, the mean and variance of the Gaussian distribution was estimated by the kriging estimate and the kriging variance. The requirements for this algorithm were a prior decision of stationarity and a variogram model. The resulting L simulated realizations honored both the data and the variogram model [*Remy et al.*, 2008]. In this paradigm, the prior belief for the Y(u) field was intended to statistically distributed as a multivariate normal distribution with a mean of point-wise arithmetic average of L simulated realizations $\langle Y(u) \rangle$ and an empirical covariance structure $C_Y(u)$.

3.3.3. MCMC Simulations

Given the prior information and the likelihood function, a large collection of *Y(u)* values, $\{Y(u)^{(1)},...,Y(u)^{(s)}\}$ was constructed to obtain the Monte Carlo approximation to the posterior distribution of *Y(u)*.

As stated earlier, the Metropolis algorithm was implemented in this study. The basic intuition behind the Metropolis algorithm is that for any two different values $Y(u)_a$ and $Y(u)_b$ we have (Equation 3.4)

$$\frac{\#\{Y(u)^{(s)}\text{'s in the collection} = Y(u)_a\}}{\#\{Y(u)^{(s)}\text{'s in the collection} = Y(u)_b\}} \approx \frac{p(Y(u)_a \mid h_0)}{p(Y(u)_b \mid h_0)} \tag{3.4}$$

Therefore adding a new value $Y(u)^*$ (proposed value) to the collection depends on the comparison of $p(Y(u)^* \mid h_0)$ to $p(Y(u)^{(s)} \mid h_0)$. The comparison can be made through computing the acceptance ratio (*r*) [*Hoff*, 2009] (Equation 3.5) :

$$\begin{aligned} r &= \frac{p(Y(u)^* \mid h_0)}{p(Y(u)^{(s)} \mid h_0)} = \frac{p(h_0 \mid Y(u)^*)\pi(Y(u)^*)}{p(h_0)} \frac{p(h_0)}{p(h_0 \mid Y(u)^{(s)})\pi(Y(u)^{(s)})} \\ &= \frac{p(h_0 \mid Y(u)^*)\pi(Y(u)^*)}{p(h_0 \mid Y(u)^{(s)})\pi(Y(u)^{(s)})} \end{aligned} \tag{3.5}$$

If $r > 1$, $Y(u)^*$ is accepted into the set since $Y(u)^*$ has a higher probability than $Y(u)^{(s)}$; and if $r < 1$, the relative frequency of *Y(u)* values in the set equal to $Y(u)^*$, compared to those equal to $Y(u)^{(s)}$ should be $\frac{p(Y(u)^* \mid h_0)}{p(Y(u)^{(s)} \mid h_0)} = r$ [*Hoff*, 2009]. The proposed variable $Y(u)^*$ is sampled from a symmetric proposal distribution $J(Y(u)^* \mid Y(u)^{(s)}) = uniform(Y(u)^{(s)} - \delta, Y(u)^{(s)} + \delta)$ with high probability being near $Y(u)^{(s)}$. In summary, the procedure implemented in this study can be described as follows:

1. Parameters were initialized at some value ($Y(u)^{(1)}$). Theoretically, vector $Y(u)$ can be initialized by any number. In this study, we chose one of the realizations of the SGSIM and added noise to each component to make it perturbed.
2. $Y(u)^{*} \sim J(Y(u)|\, Y(u)^{(s)})$ was sampled by drawing a value $Y(u)^{*}$ from the uniform distribution $(Y(u)^{(s)} - \delta, Y(u)^{(s)} + \delta)$ where δ is a pre-determined small number .
3. The acceptance ratio (r) was computed. If $r>1$, we accepted $Y(u)^{*}$ into our set, i.e. $Y(u)^{(s+1)} = Y(u)^{*}$. If $r<1$ then we set $Y(u)^{(s+1)}$ equal to either $Y(u)^{*}$ or $Y(u)^{(s)}$, with probability r and $(1-r)$ respectively. This was accomplished by sampling $q \sim uniform(0,1)$ and setting $Y(u)^{(s+1)} = Y(u)^{*}$ if $q< r$ and setting $Y(u)^{(s+1)} = Y(u)^{(s)}$ otherwise [*Hoff*, 2009].
4. Steps 2 and 3 were repeated until the chain converges.

The early iterations, the so called "burn-in" period in which the Markov Chain moved from its initial value to a region of high posterior probability, were discarded.

3.4. Case Study

The numerical application of the MCMC approach to the inverse problem of a hypothetical groundwater model is demonstrated in this section. The groundwater model was constructed using MODFLOW-2000 with the domain size of 220 m in the *x*-direction and 14 m in the *z*-direction which was discretized into 10 layers and 15 columns (Figure 26) . In addition to the 150 nodes in the FD grid, the time domain consists of 100 days of transient stress periods. The same discretization was used for the SGSIM. The no-flow boundary conditions were prescribed at the left-hand side of the domain in addition to the bottom layer. Evapotranspiration and recharge boundary

conditions [*Harbaugh et al.*, 2000] were applied to the top layer and General Head Boundary (GHB) conditions [*Harbaugh et al.*, 2000] were applied to the right-hand boundary of the domain .

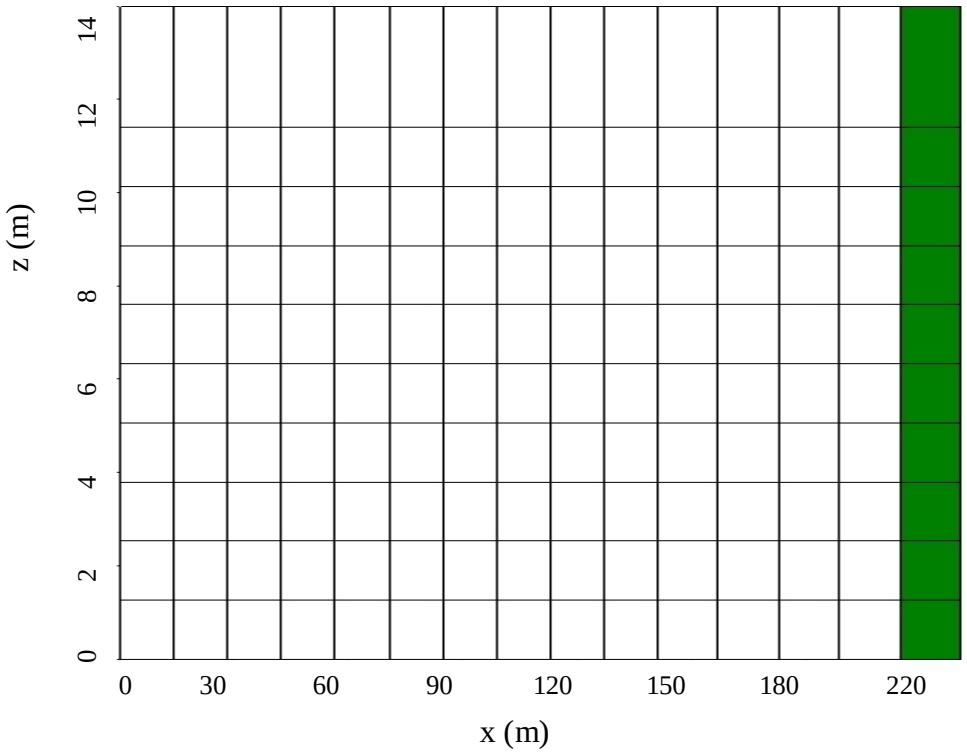

Figure 26. MODFLOW-2000 model discretization into 10 layers and 15 columns. The green column on the right represents the General Head Boundary condition .

A

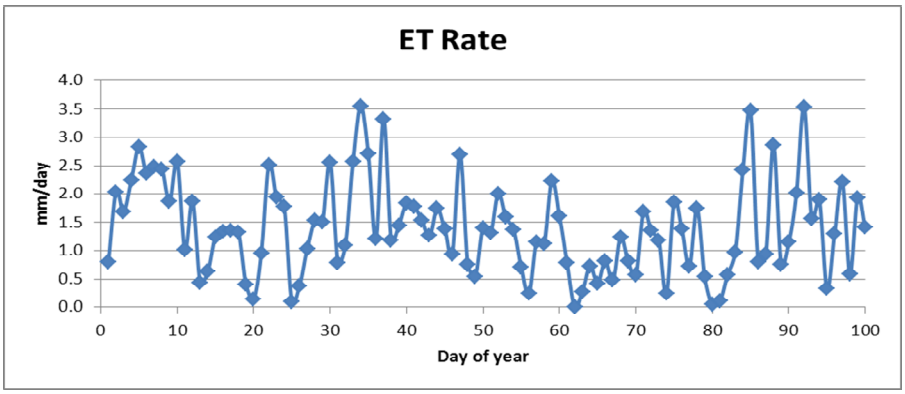

B

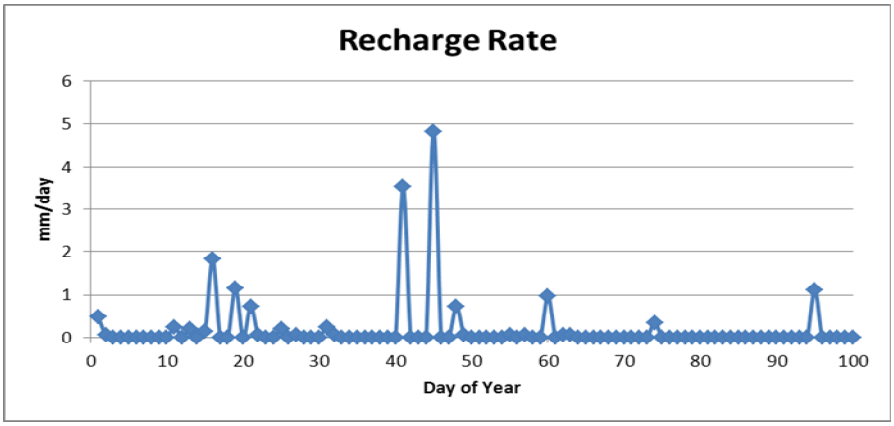

C

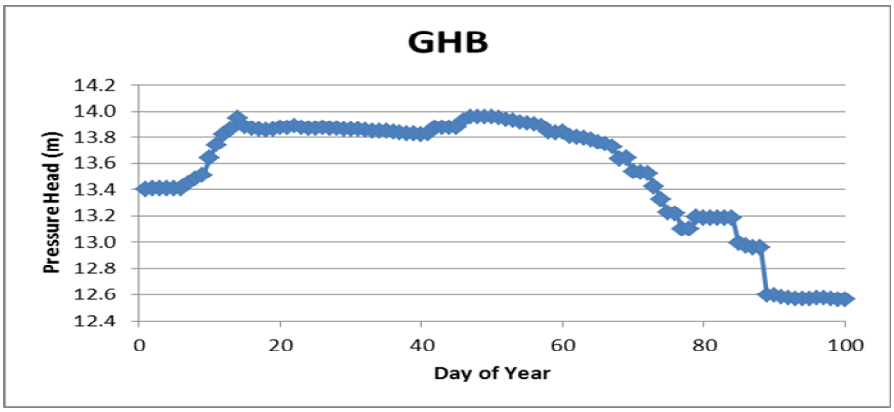

Figure 27. (A) ET rate, (B) Recharge rate and (C) General Head Boundary (GHB) condition. The Recharge and ET rate were obtained from the real measurements at the Norman Landfill site [*http://www.mesonet.org*].

The measurements of the hydraulic conductivity were adopted from the study conducted by *Scholl et al*. [1998] at the Norman Landfill site. According to *Scholl et al*.[1998], the hydraulic conductivity measurements were made using the slug test method along a 215 m flow path transect through a 11 m thick aquifer (Figure 6). The SGSIM algorithm calls for input of only 2-point statistics (variogram) and hence it cannot deliver any image with existence of definite geologic patterns or structures. [*Remy et al.*, 2008]. Due to this limitation, the clayey layers at the Norman Landfill site were excluded. In addition, the high hydraulic conductivity layer at the base of the aquifer was discarded in order to simulate a heterogeneous spatial distribution of hydraulic conductivity within a homogeneous lithoface. The changes in the actual field were made to provide the stationary condition.

Figure 28 shows the variability of the data in the field and Figure 29 and Figure 30 are the histogram and quantile-quantile plots to check for any significant deviations from normality.

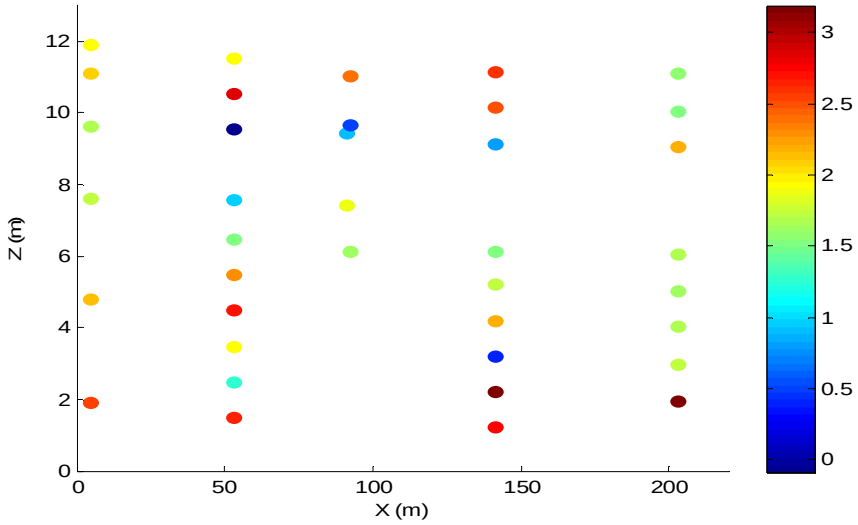

Figure 28. Profile map of the log hydraulic conductivity measurement (m/day) distributed throughout the field.

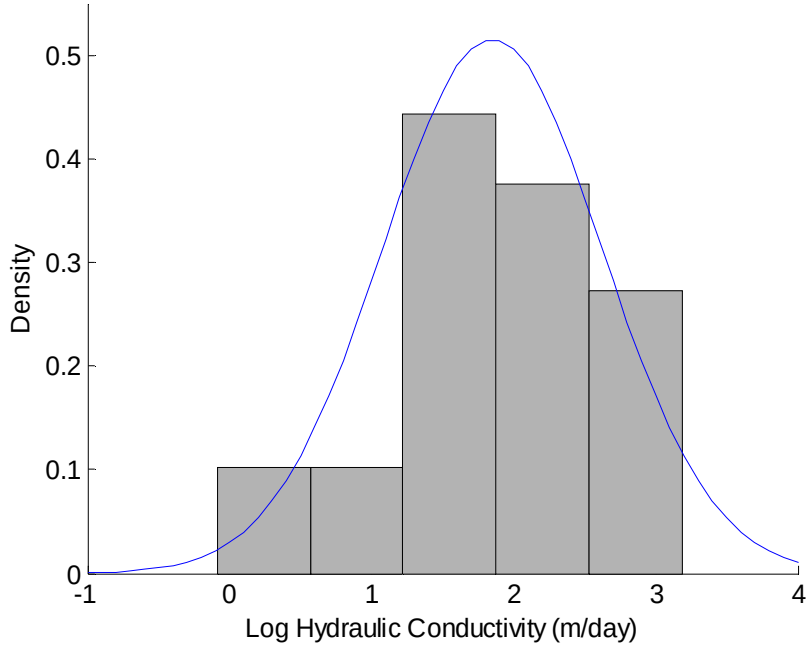

Figure 29. Relative histogram of the measured Log hydraulic conductivity data (m/day) with a normal density superimposed . Data count number is 38 with the mean of 1.85 and variance of 0.55.

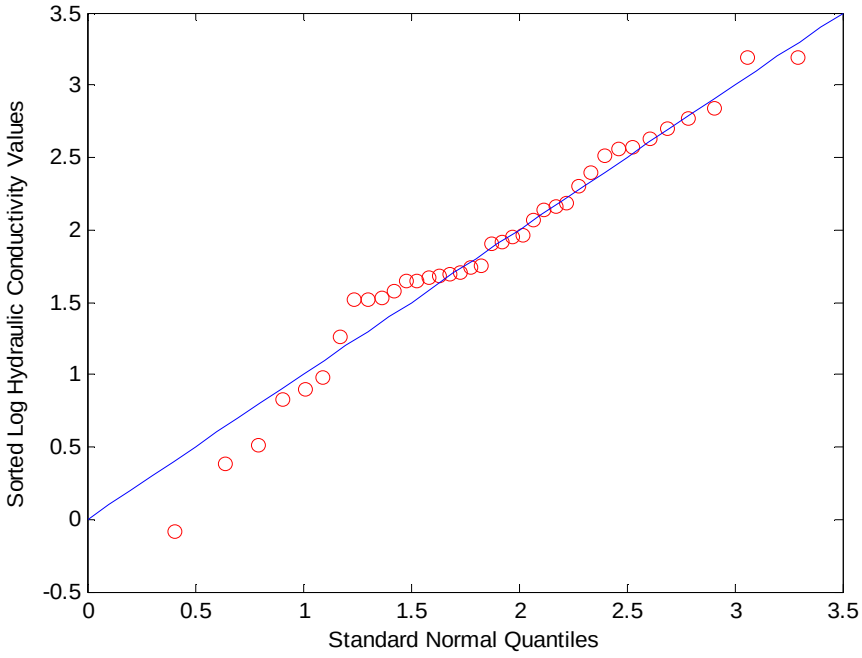

Figure 30. Normal quantile-quantile plot- shows that the log hydraulic conductivity does not deviate too severely from normality

The semivariogram model used in the stochastic simulation consists of a nugget of 0.0 , a Gaussian component with a maximum range of 12.6 and a sill of 0.52 (Figure 31)

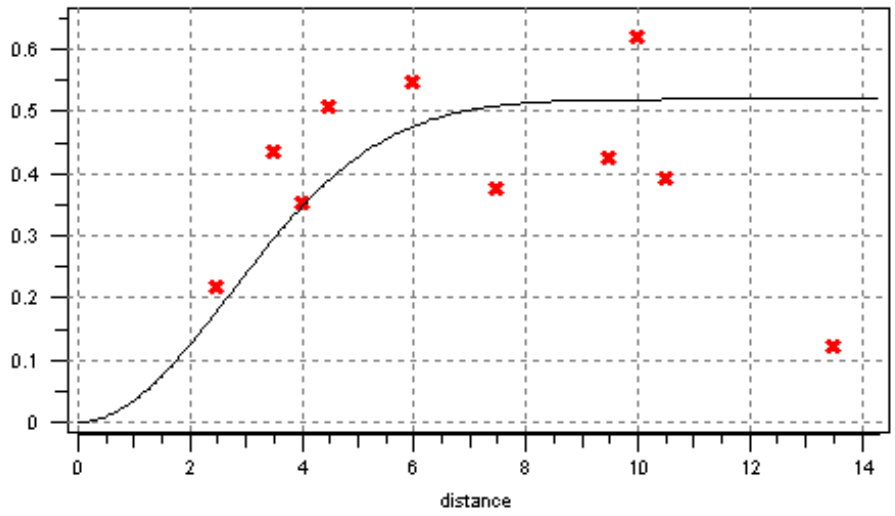

Figure 31. The empirical semivariogram (red x) and the semivarigram model (black line) of the log hydraulic conductivity with azimuth= 90 and dip=0.

At first, a random field using the specified variogram model was generated by means of the SGSIM and considered the "true" field (reference field, Figure 32). The reference field was estimated later using the proposed inverse procedure.

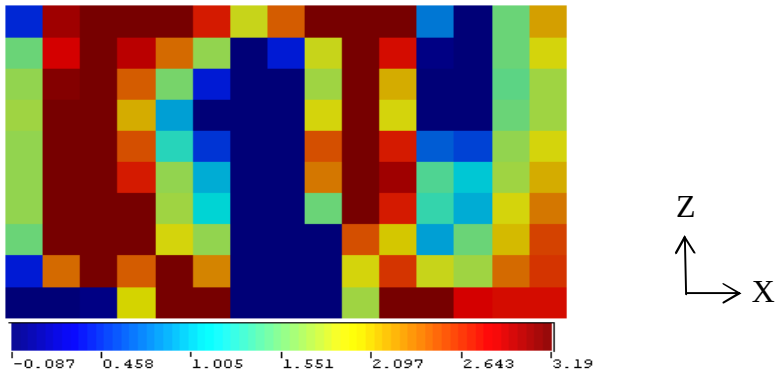

Figure 32. Reference log (K) field. (m/day)

Using the reference field, direct measurements of the hydraulic head at one location (middle column, top layer) were taken for the whole period of transient flow simulation (h_0) (Figure 33).

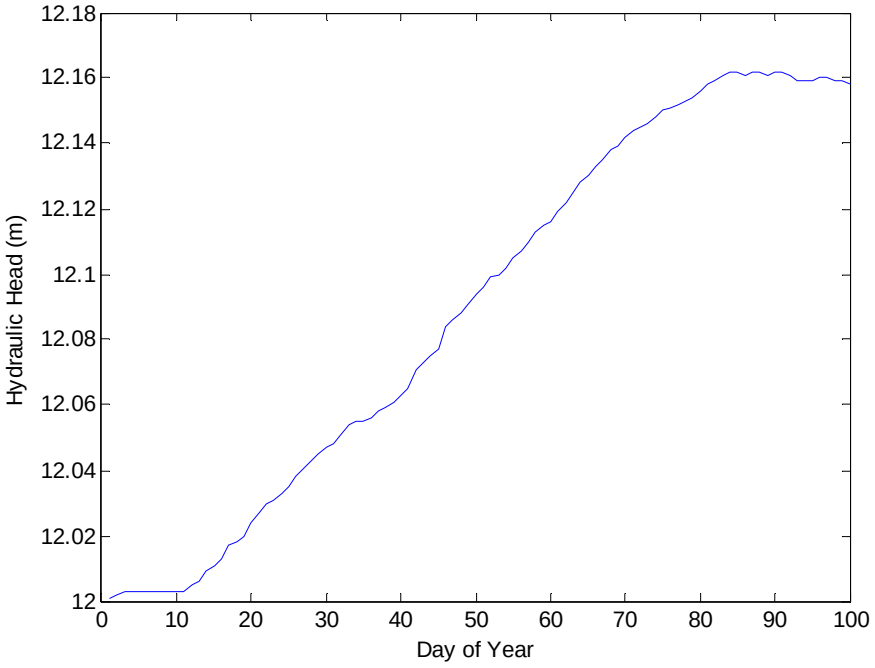

Figure 33. Hypothetical hydraulic head measurements for 100 days of transient flow simulation. (location of observation: top layer, middle column)

1000 realizations were generated using SGSIM and the ensemble statistics were taken as the prior mean and the prior covariance. Figure 34 shows a few samples from the 1000 realizations :

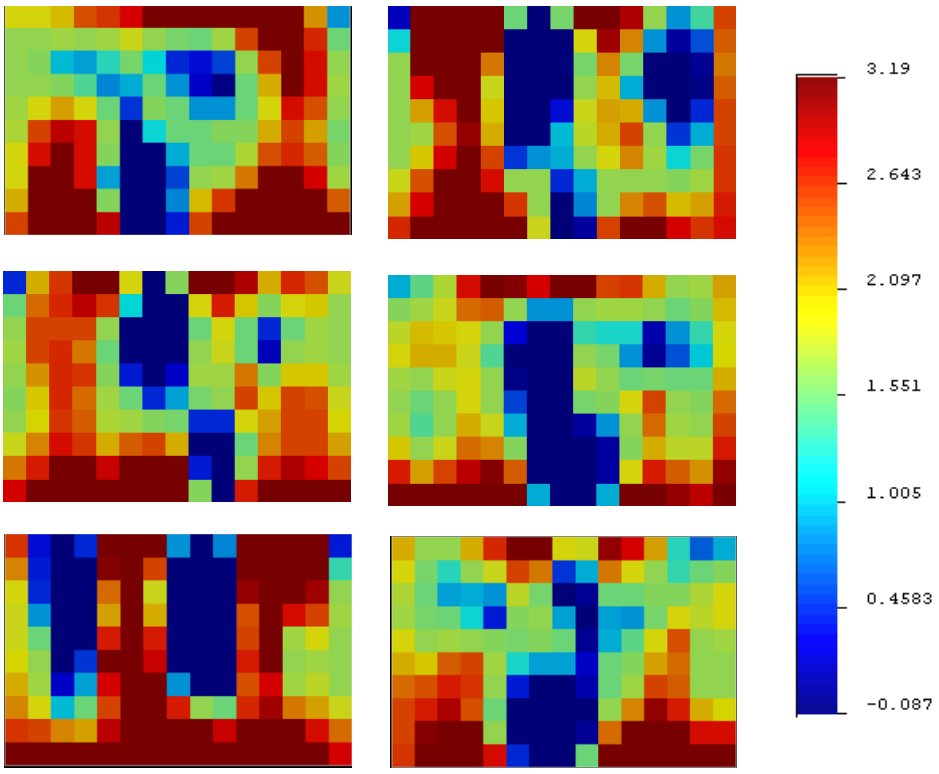

Figure 34. Six samples out of thousand realizations of the log hydraulic conductivity field. (m/day)

The prior mean and prior covariance structure are illustrated in Figure 35.

A

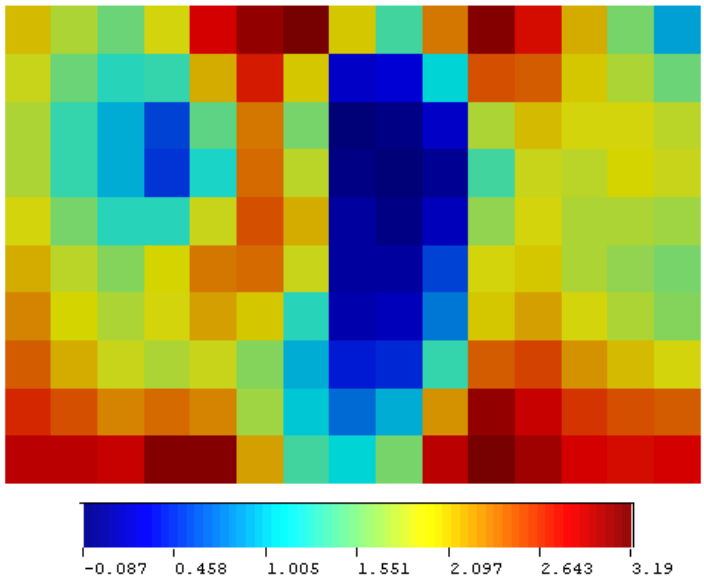

B

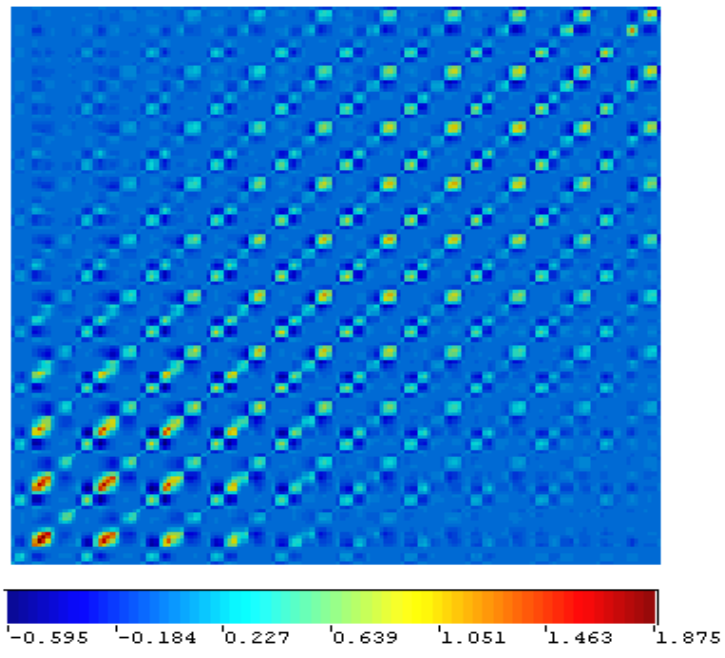

Figure 35. (A) Prior mean of log hydraulic conductivity (m/day) and (B) Prior covariance structure.

3.5. Results and Discussion

Using the Metropolis algorithm, 1000 values of log (K) for each grid cell were generated $\{Y(u)^{(1)},...,Y(u)^{(1000)}\}$ with the average acceptance ratio of 0.10 . The Monte Carlo approximation to the posterior density of the $Y(u)$ for the first four grid cells of column one are illustrated in Figure 36.

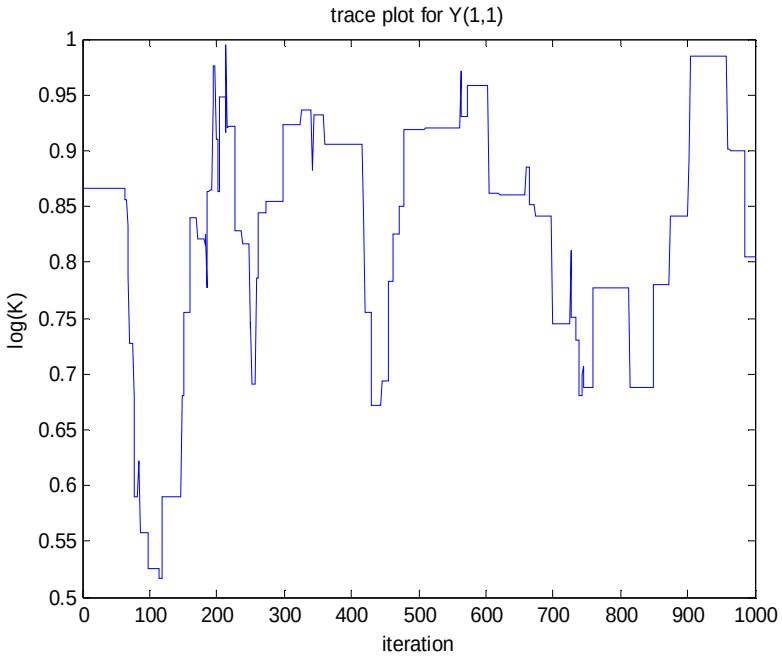

A

Figure 36. Trace plots for the first four grid cells of the first column.

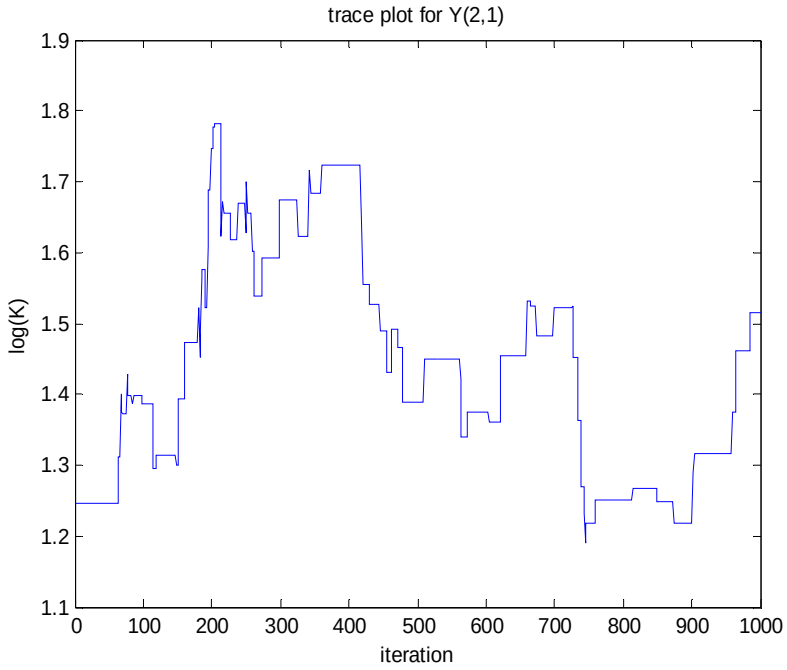

B

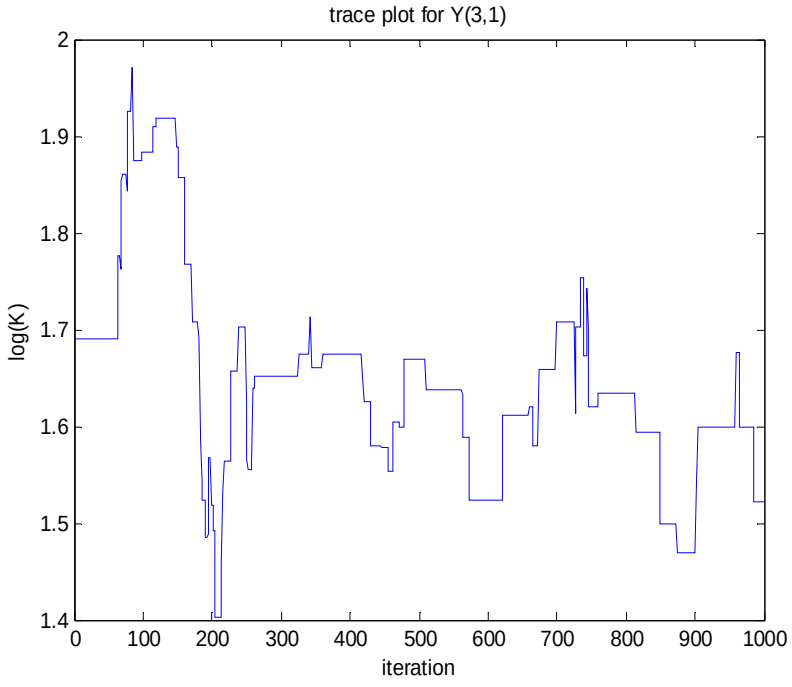

C

Figure 36. Continued.

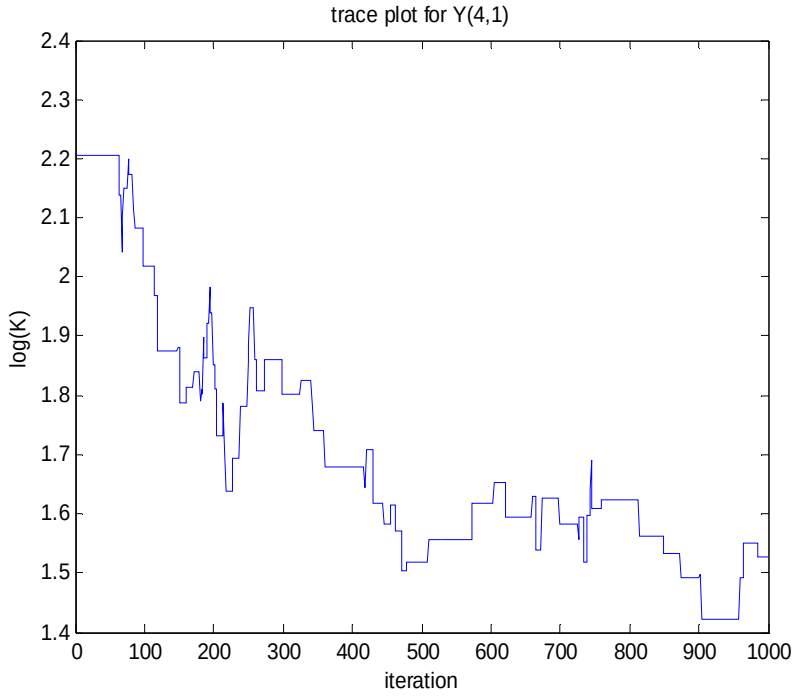

D

Figure 36. Continued.

The above trace plots indicate that the chain for each variable got stuck for long periods indicating a low acceptance ratio. Proposals were accepted for only 10% of the iterations, and so $Y(u)^{(s+1)}$ were set equal to $Y(u)^{(s)}$ 90% of the time , resulting in a highly correlated Markov chain. In order to alleviate the burden of highly correlated Markov chain, only a fraction of the scans of the Markov chain were saved. This practice of throwing away part of iterations of a Markov chain is common and referred to as thinning [*Hoff*, 2009] .

The effect of the Markov chain on the hydraulic head at the observation point is an implicit measure of estimation accuracy. Figure 37 illustrates the hydraulic head simulations in which only every 10^{th} iteration of 1000 sequential samples was selected

(black asterisks are the “truth” hypothetical observation points). The color bar represents the order of thinned iterations from blue as the first iteration to red as the last one. Figure 37 clearly shows that the hydraulic head simulations improved through the inversion method.

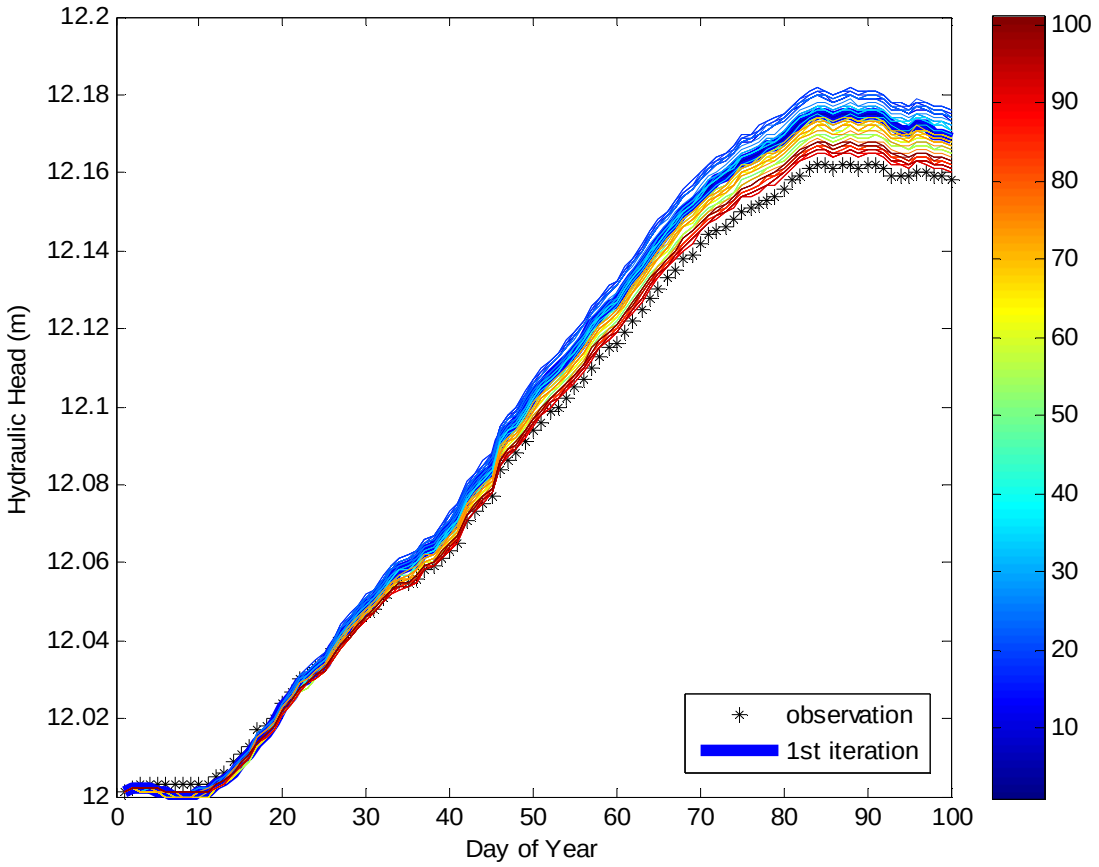

Figure 37. Hydraulic head simulations for 100 iterations and the “true” hypothetical observation points.

Figure 38(a) shows the estimated log hydraulic conductivity field and Figure 38 (b) shows the true versus estimated log hydraulic conductivity values with correlation coefficient of 0.67 and root mean squared error of 1.67 . It seems that the inverse model

performance was relatively good for the mid-values of $Y(u)$ but not good at the extrema as shown in Figure 38(b).

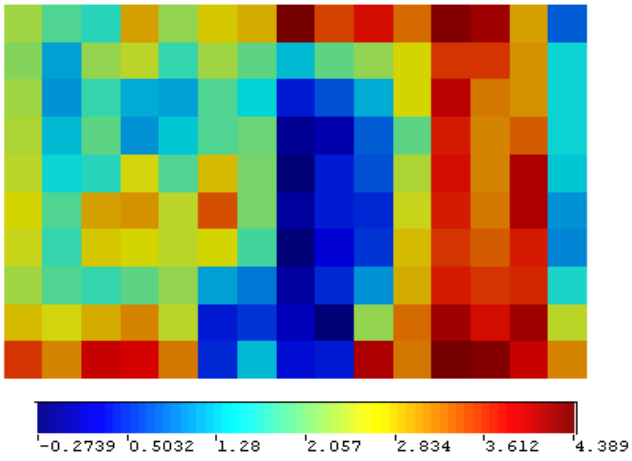

A

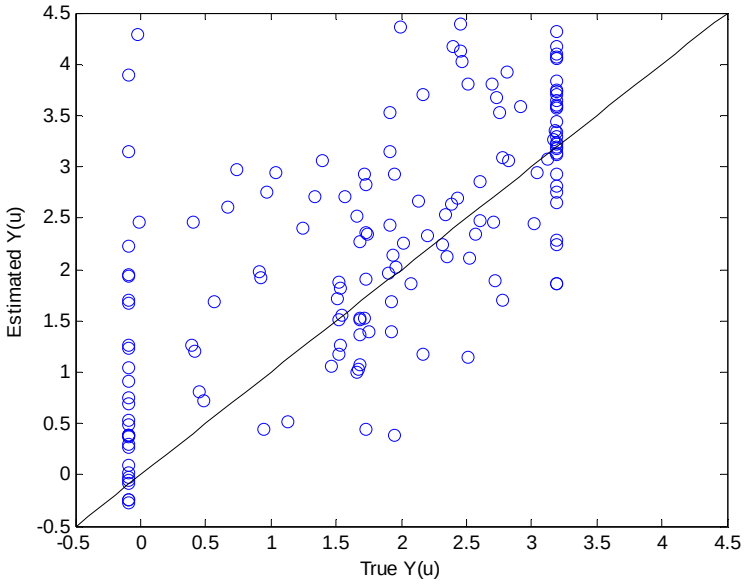

B

Figure 38. (A) Estimated log hydraulic conductivity (m/day) (B) Estimated versus true log hydraulic conductivity values

The key source of uncertainty in this study is the simplifying assumptions that were made to conduct the MCMC scheme. These assumptions include normality of the log (K) field for calculating the prior covariance matrix using the empirical covariance function and also stationarity for obtaining the variogram model.

Another source of uncertainty comes from the way the parameters were updated in the MCMC framework. In the proposed method, the components of the Y(u) were updated all together to expedite the generation of the Markov chain which is unlike the Metropolis rule to update the components of Y(u) one at a time.

4. CONCLUSIONS

In the light of the results from the numerical simulation of the Norman Landfill site, the following conclusions can be derived. The analysis showed that the hydraulic conductivity and the specific yield play an important role in water table fluctuations through storage but the general trend of the water table is controlled by the recharge and ET rate at the Norman Landfill. Soil properties are dominant factors in controlling the amplitude of the rise in the water table due to rain events. The structure of soil properties presented here cannot be unique solutions for the model. By utilizing PEST, hundreds of scenarios of hydraulic conductivity, specific yield and recharge patterns were tested for the optimum calibration simulation and to represent the processes occurring in the field. The constraints imposed on the model parameters were based on field measurements and earlier studies at the site or other similar sites. The hydrologic regime of the wetland is governed by its relationship to climate, soil and vegetation dynamics as well as its interconnection with the aquifer. The model was successfully used to understand the relative contributions of different hydrological processes in the wetland such as groundwater inflow, outflow and ET.

During the transient calibration it was identified that in order to reproduce the observed groundwater levels, recharge multiplier would be divided into different zones with each individual zone having its own characteristics.. Results from the numerical model suggest the range of 23% to 84% as the recharge multiplier for the domain. The recharge values have distinct seasonal patterns especially for the mound area. *Cozzarelli et al.* [2000]observed that leachate contaminated groundwater discharges to the wetland

along the northeast bank and that wetland water recharges to the aquifer along the southwest bank [*Cozzarelli et al.*, 2000]. Following this observation the model dealt with a flow-through wetland by considering the specific ratio of K_x/K_z. Model results indicate that the wetland is fed by the groundwater flow but it could not precisely quantify the outflow from the wetland. This could be a serious modeling challenge in the surface water- groundwater interaction but does not undermine the validation of the model.

Comparisons of simulated and observed water levels are valuable for evaluating the limitations of the model. The discrepancies between the total inflow and out-flow from the water budget analysis were helpful to assess whether the model does or does not account for important processes. Uncertainties related to recharge and specific yield have to be included in order to assess if mass balance calculations resulted in erroneous quantification of groundwater inflow/outflow. Without uncertainty analysis it is difficult to draw a definite conclusion.

In this part of the study we quantified the water balance components in the aquifer-wetland system at the Norman Landfill site. Important hydrological processes were quantified such as the inflow, outflow, recharge and ET rates also the rate and volume of groundwater entering the wetland. These are the necessary components to evaluate the surface water – groundwater interactions. Model results of the response of an aquifer-wetland system to climate, soil and vegetation were useful to understand the intensity and duration of groundwater recharge, differences in ET rates between the mound, riparian area and the wetland.

The results from the second study demonstrated that the MCMC method captured the structure of the reference field only for the mid-values of the hydraulic conductivities which implies that the inverse model has not reached a desired level of maturity. In this study we worked with a covariance matrix of high dimension. Calculating the prior covariance matrix becomes computationally prohibitive as the size of the matrix increases. In addition, increasing the size of the covariance matrix may decrease its precision. The MCMC scheme has been proved to be applicable to covariance matrix of high dimension [*Smith et al.*, 2002]. Therefore we can conclude that the robustness of the inverse model depends on the precision of the covariance matrix.

The hypothetical example is a special study to test the groundwater inverse modeling for the reason that the reference field is already defined. Since the reference field of the hydraulic conductivity is available, comparison between the estimation and the "truth" state can be made. However, in reality, the variability of hydraulic conductivity in the field can never be known with certainty and the performance of the inverse model would depend only on the matching between the simulated and measured dependent variables. Therefore, the model's ability to improve the simulation of the dependent variable is considered as the measure of model accuracy. The simulation result in this study demonstrated that the transient head simulations favorably improved through the inverse model.

REFERENCES

Ajami, H., T. Maddock, T. Meixner, J. F. Hogan, and D. P. Guertin (2012), RIPGIS-NET: A GIS Tool for riparian groundwater evapotranspiration in MODFLOW, *Ground Water*, *50*(1), 154-158.

Arnold, J. G., P. M. Allen, and G. Bernhardt (1993), A comprehensive surface-groundwater flow model, *Journal of Hydrology*, *142*(1), 47-69.

Baez-Cazull, S. E., J. T. McGuire, I. M. Cozzarelli, and M. A. Voytek (2008), Determination of dominant biogeochemical processes in a contaminated aquifer-wetland system using multivariate statistical analysis, *Journal of Environmental Quality*, *37*(1), 30-46.

Banta, E. R. (2000), MODFLOW-2000, The US Geological Survey Ground-water Modular Model—Documentation of packages for simulating evapotranspiration with a segmented function (ETS1) and drains with return flow (DRT1) *Rep. 00-466*, U.S Geological Survey, Denver, Colorado.

Becker, C. J. (2002), Hydrogeology and leachate plume delineation at a closed municipal landfill, Norman, Oklahoma *Rep. 01-4168*, US Department of the Interior, US Geological Survey.

Belmans, C., J. G. Wesseling, and R. A. Feddes (1983), Simulation model of the water balance of a cropped soil: SWATRE, *Journal of Hydrology*, *63*(3-4), 271-286.

Bowles, D. S., and P. E. O'Connell (1991), *Recent advances in the modeling of hydrologic systems (NATO Science Series C: (closed))*, Kluwer Academic Publishers, Netherlands.

Burgess, L. J. (2006), Vascular flora of a riparian site on the Canadian River, Cleveland County, Oklahoma *Rep. 1*, University of Oklahoma, Norman.

Busch, D. E., N. L. Ingraham, and S. D. Smith (1992), Water uptake in woody riparian phreatophytes of the southwestern United States: a stable isotope study, *Ecological Applications*, *2*(4), 450-459.

Carrera, J., A. Alcolea, A. Medina, J. Hidalgo, and L. J. Slooten (2005), Inverse problem in hydrogeology, *Hydrogeology Journal*, *13*(1), 206-222.

Carter, V. (1996), Wetland hydrology, water quality, and associated functions *Rep. 2425*, 35-48 pp, U.S Department of the Interior ; U.S. Geological Survey, Washington, D.C.

Chen, J., S. Hubbard, and Y. Rubin (2001), Estimating the hydraulic conductivity at the South Oyster Site from geophysical tomographic data using Bayesian techniques based on the normal linear regression model, *Water Resources Research*, *37*(6), 1603-1613.

Christenson, S., and I. Cozzarelli (2003), The Norman Landfill environmental research site: What happens to the waste in landfills?, edited, U.S. Geological Survey Fact sheet FS-040-03,1-4.

Christenson, S., M. A. Scholl, J. L. Schlottman, and C. J. Becker (1999), Ground-water and surface-water hydrology of the Norman Landfill Research Site, paper presented at U.S. Geological Survey -Toxic Substances Hydrology Program, U.S. Geological Survey, Charleston, South Carolina, March 8-12.

Copty, N., and Y. Rubin (1995), A stochastic approach to the characterization of lithofacies from surface seismic and well data, *Water Resources Research*, *31*(7), 1673-1686.

Cosner, O. J., and F. J. Harsh (1978), Digital-model simulation of the glacial-outwash aquifer, Otter Creek-Dry Creek basin, Cortland County, New York *Rep. 78-71*, U.S. Geological Survey.

Cozzarelli, I. M., J. M. Suflita, G. A. Ulrich, S. H. Harris, M. A. Scholl, J. L. Schlottmann, and S. Christenson (2000), Geochemical and microbiological methods for evaluating anaerobic processes in an aquifer contaminated by landfill leachate, *Environmental Science & Technology*, *34*(18), 4025-4033.

Dagan, G. (1986), Statistical theory of groundwater flow and transport: pore to laboratory, laboratory to formation, and formation to regional scale, *Water Resources Research*, *22*(9S), 120S-134S.

Deutsch, C. V., and A. G. Journel (1998), *GSLIB: Geostatistical software library and user's guide*, Oxford University Press New York.

Doherty, J. (2004), *PEST: Model-Independent Parameter Estimation User Manual*, Watermark Numerical Computing, Brisbane, Australia.

Domenico, P. A. (1972), *Concepts and models in groundwater hydrology*, McGraw-Hill New York.

Doss, P. K. (1993), The nature of a dynamic water table in a system of non-tidal, freshwater coastal wetlands, *Journal of Hydrology*, *141*(1-4), 107-126.

Eagleson, P. (1978), Climate, soil, and vegetation: 1. Introduction to water balance dynamics, *Water Resources Research*, *14*(5), 705-712.

Eganhouse, R. P., L. L.Matthews, I. M. Cozzarelli, and M. A. Scholl (1999), Evidence of natural attenuation of volatile organic compounds in the leachate plume of a municpal landfill near Norman,Oklahoma, paper presented at U.S. Geological Survey- Toxic Substance Hydrology Program, Charleston, South Carolina, March 8-12.

Eggleston, J., and S. Rojstaczer (1998), Identification of large-scale hydraulic conductivity trends and the influence of trends on contaminant transport, *Water Resources Research*, 2155-2168.

Ezzedine, S., Y. Rubin, and J. Chen (1999), Bayesian method for hydrogeological site characterization using borehole and geophysical survey data: Theory and application to the Lawrence Livermore National Laboratory Superfund site, *Water Resources Research*, *35*(9), 2671-2683.

Gelhar, L. W. (1986), Stochastic subsurface hydrology from theory to applications, *Water Resources Research*, *22*(9S), 135S-145S.

Gill, P. E., and W. Murray (1978), Algorithms for the solution of the nonlinear least-squares problem, *SIAM Journal on Numerical Analysis*, *15*(5), 977-992.

Ginn, T., and J. Cushman (1990), Inverse methods for subsurface flow: A critical review of stochastic techniques, *Stochastic Hydrology and Hydraulics*, *4*(1), 1-26.

Hadamard, M. (1902), On problems in partial derivatives, and their physical significance, *Princeton University Bulletin*, *13*, 82-88.

Harbaugh, A., E. Banta, M. Hill, and M. McDonald (2000), MODFLOW-2000, the USGS modular ground-water model-user guide to modularization concepts and the ground-water flow process *Rep. 00-92*, U.S. Geological Survey.

Hoff, P. D. (2009), *A first course in bayesian statistical methods*, Springer Verlag.

http://modis.gsfc.nasa.gov National Aeronautics and Space Administration-Goddard Space Flight Center, Accessed May 13 2010.

http://ok.water.usgs.gov/projects/norlan/ Substances Hydrology Program - Norman Landfill Project, edited, U.S. Department of the Interior ,U.S. Geological Survey, Accessed June 1 2010.

Jordan, C. F. (1969), Derivation of leaf-area index from quality of light on the forest floor, *Ecology*, *50*(4), 663-666.

Journel, A. G. (1989), *Fundamentals of geostatistics in five lessons*, American Geophysical Union, USA.

Journel, A. G. (1993), *Geostatistics: roadblocks and challenges*, 213-224 pp., Kluwer Academic, Dordrech.

Kitanidis, P. K. (1996), On the geostatistical approach to the inverse problem, *Advances in Water Resources*, *19*(6), 333-342.

Kitanidis, P. K., and E. G. Vomvoris (1983), A geostatistical approach to the inverse problem in groundwater modeling (steady state) and one-dimensional simulations, *Water Resources Research*, *19*(3), 677-690.

Lindgren, R. J., and M. K. Landon (1999), Effects of ground-water withdrawals on the Rock River and associated valley aquifer, eastern Rock County, Minnesota *Rep. 98-4157* US Geological Survey, USA.

Lu, Z., D. M. Higdon, and D. Zhang (2004), A Markov Chain Monte Carlo method for the groundwater inverse problem, paper presented at The XVth International Conference on Computational Methods in Water Resources, Los Alamos, New Mexico.

Madsen, H. (2000), Automatic calibration of a conceptual rainfall–runoff model using multiple objectives, *Journal of Hydrology*, *235*(3–4), 276-288.

Markstrom, S. L., R. G. Niswonger, R. S. Regan, D. E. Prudic, and P. M. Barlow (2008), *GSFLOW- coupled ground-water and surface-water flow model based on the integration of the precipitation-runoff modeling system (PRMS) and the modular ground-water flow model (MODFLOW-2005)* US Geological Survey, Reston, Virginia.

Marston, R. A., and S. T. Paxton (2001), Geomorphology and sedimentology of the Canadian River alluvium adjacent to the Norman Landfill, Norman, Oklahoma *Rep.*, 74 pp, Stillwater, Oklahoma.

Masoner, J. R., D. I. Stannard, and S. C. Christenson (2008), Differences in evaporation between a floating pan and class A pan on land, *JAWRA Journal of the American Water Resources Association*, *44*(3), 552-561.

McDonald, M. G., and A. W. Harbaugh (1998), User's documentation for MODFLOW-96, an update to the U.S. Geological Survey modular finite-difference ground-water flow model *Rep. 96-485*, 56 pp, U.S. Geological Survey, USA.

McLaughlin, D., and L. R. Townley (1996), A reassessment of the groundwater inverse problem, *Water Resources Research*, *32*(5), 1131-1161.

Merritt, M. L., and L. F. Konikow (2000), Documentation of a computer program to simulate lake-aquifer interaction using MODFLOW ground-water flow model and the MOC3D solute-transport model *Rep. 00-4167*, U.S. Geological Survey, Tallahassee, Florida.

Metropolis, N., A. W. Rosenbluth, M. N. Rosenbluth, A. H. Teller, and E. Teller (1953), Equation of state calculations by fast computing machines, *Journal of Chemical Physics*, *21*(6), 1087.

Nachabe, M. (2002), Analytical expressions for transient specific yield and shallow water table drainage, *Water Resources Research*, *38*(10), 1193.

Neuman, S. P. (1973), Calibration of distributed parameter groundwater flow models viewed as a multiple-objective decision process under uncertainty, *Water Resources Research*, *9*(4), 1006-1021.

NWS Internet Services Team National Oceanic and Atmospheric Administration's, edited, National Weather Service, Accessed May 2 2010.

Press, W. H., S. A. Teukolsky, W. T. Vetterling, and B. P. Flannery (1992), *Numerical Recieps in Fortran: The Arth of Scientific Computing*, Cambridge University Press, New York, USA.

Purdic, D. (1989), Documentation of a computer program to simulate stream-aquifer relations using a modular finite-difference ground-water flow model *Rep. 88-729*, US Geological Survey, Denver.

Remy, N., A. Boucher, and J. Wu (2008), *Applied geostatistics with SGeMS: A user's guide*, Cambridge University Press, New York, USA.

Schlottmann, J. L., M. A. Scholl, and I. M. Cozzarelli (1999), Identifying ground-water and evaporated surface-water interactions near a landfill using Deutriuum, Oxygen and Chloride, Norman,Oklahoma, paper presented at U.S. Geological Survey Toxic Substances Hydrology Program, U.S. Geological Survey Charleston, South Carolina, March 8-12, 1999.

Schlumberger Water Services, and Waterloo Hydrogeologic Incorporation (2010), Visual MODFLOW Pro. 3D Groundwater Flow and Contaminant Transport Modeling edited.

Scholl, M., I. M. Cozzarelli, S. Christenson, G. N.Breit, and J. L. Schlottmann (1999), Aquifer heterogeneity at the Norman Landfill and its effect on observations of biodegradation processes, paper presented at U.S.Geological Survey-Toxic Substance Hydrology Program, USGS, Charleston, South Carolina, March8-12.

Scholl, M. A., and S. Christenson (1998), Spatial variation in hydraulic conductivity determined by slug tests in the Canadian River alluvium near the Norman Landfill, Norman , Oklahoma *Rep. 97-4292*, U.S Department of the Interior- U.S. Geological Survey, Oklahoma City.

Scholl, M. A., I. M. Cozzarelli, and S. C. Christenson (2006), Recharge processes drive sulfate reduction in an alluvial aquifer contaminated with landfill leachate, *Journal of Contaminant Hydrology*, 239-261.

Simunek, J., M. Sejna, and M. T. v. Genuchten (1998), The HYDRUS-1D software package for simulating the movement of water, heat, and multiple solutes in variably saturated media, version 2.0 *Rep.*, U.S Salinity Laboratory, Reverside , California.

Smith, M., and R. Kohn (2002), Parsimonious covariance matrix estimation for longitudinal data, *Journal of the American Statistical Association*, *97*(460), 1141-1153.

Sun, N. Z., and W. W. G. Yeh (1990), Coupled inverse problems in groundwater modeling 1. Sensitivity analysis and parameter identification, *Water Resources Research*, *26*(10), 2507-2525.

Todd, D. K., and L. W. Mays (2005), *Groundwater Hydrology*, 3 ed., John Wiley & Sons, Inc., USA.

Twarakavi, N. K. C., J. Simunek, and S. Seo (2008), Evaluating interactions between groundwater and vadose zone using the HYDRUS-based flow package for MODFLOW, *Vadose Zone Journal*, 757-768.

Winter, T. (1999), Relation of streams, lakes, and wetlands to groundwater flow systems, *Hydrogeology Journal*, 28-45.

Winter, T. C. (1976), Numerical simulation analysis of the interaction of lakes and ground water *Rep. 323943*, U.S. deptartment of the interior, Washington.

Woodbury, A. D., and T. J. Ulrych (2000), A full-Bayesian approach to the groundwater inverse problem for steady state flow, *Water Resources Research*, *36*(8), 2081-2093.

Wu, K., N. Nunan, J. W. Crawford, I. M. Young, and K. Ritz (2004), An efficient Markov chain model for the simulation of heterogeneous soil structure, *Soil Science Society of America Journal*, *68*(2), 346-351.

www.mesonet.com (1994), The Oklahoma Mesonet website, edited, Board of Regents of the University of Oklahoma, Accessed May 2 2010.

Yeh, T. C. J., A. L. Gutjahr, and M. Jin (1995), An iterative cokriging like technique for ground-water flow modeling, *Ground Water*, *33*(1), 33-41.

Yeh, W. W. G. (1986), Review of parameter identification procedures in groundwater hydrology: The inverse problem, *Water Resources Research*, *22*(2), 95-108.

Zheng, C., and G. D. Bennet (2002), *Applied Contaminant Transport Modeling*, 2 ed., John Wiley & Sons Inc., New York.

VITA

Sayena Farid Marandi received her Bachelor of Engineering degree in water resources from The Iran University of Science and Technology in 2005. She entered the Water program at Texas A&M University in January 2009 and changed her Major to Biological and Agricultural Engineering in 2010. Her research interests include groundwater modeling and inverse modeling.

Ms. Farid Marandi may be reached at Texas A&M University, Biological & Agricultural Engineering Department, 232 Scoates Hall #2117, College Station TX 77843-2117 . Her email is sayena79@gmail.com.